Reducing DC-Link Capacitance Requirements in Large Wind Turbines

Electrical and Electronic Engineering

By

MO AL-AKAYSHEE

Department of Engineering
UNIVERSITY OF BRISTOL

A dissertation submitted to the University of Bristol in accordance with the requirements of the degree of MASTER OF SCIENCE BY RESEARCH in the Faculty of Engineering.

DECEMBER 2018

Word count: 12,000 Words

ABSTRACT

The thesis aims to determine a practical method to reduce the DC-Link voltage ripple in large wind turbines. Various wind energy conversion system configurations have been discussed and analysed in the literature review. One of the key issues found are the requirement for devices to be connected in series in order to attain the high voltages of large wind turbines.

A multi-level modular topology has been presented and analysed in detail, simulation results showing the topology operating as part of a wind energy conversion system for a large wind turbine have been presented and discussed. Experimental results have also been produced in a lab enviroment using scaled down voltages and currents. The control system was developed digitally and implemented using a DSP and CPLD board. The topology is able to overcome the issues of connecting devices in series by providing a modular structure which is inherently fault tolerant, and able to reach the high voltages required without connecting devices in series (for a single power switch).

Further work has been carried out in order to simplify the control complexity of the system, by reducing the number of active switching components. Simulation results have been presented for this, both as a standalone converter and in the wind energy conversion system in order to validate its feasibility.

Dedication and acknowledgements

I would like to take this opportunity to thank my supervisor Xibo Yuan for his patience and support over the years, both academically and personally.

To my family and close friends, your belief in my ability and sacrifices you have made it possible for me to get this far. For that I am forever grateful.

Author's declaration

I declare that the work in this dissertation was carried out in accordance with the requirements of the University's Regulations and Code of Practice for Research Degree Programmes and that it has not been submitted for any other academic award. Except where indicated by specific reference in the text, the work is the candidate's own work. Work done in collaboration with, or with the assistance of, others, is indicated as such. Any views expressed in the dissertation are those of the author.

SIGNED: Mo Al-Akayshee DATE: 14/12/2018

TABLE OF CONTENTS

List of Tables

Table **Page**

List of Figures

Figure **Page**

Abbreviations

List of abbreviations:

WECS = Wind energy conversion system
DFIG = Doubly fed induction generator
PMSM = Permanent Magnet Synchronous Machines
NPC = Neutral Point Clamped
NPP = Neutral Point Piloted
FCC = Flying Capacitor Converter
VSC = Voltage source converter
PWM = Pulse Width Modulation
LVRT = Low Voltage Ride Through
PFC = Power Factor Correction
PLL = Phase Locked Loop
ZDC = Zero D Axis
MPPT = Maximum Power Point Tracking
DTC = Direct Torque Control
MPTA = Maximum Torque Per Ampere
PI = Proportional-Integral

CHAPTER 1

INTRODUCTION

Due to the problems associated with fossil fuels, such as environmental impact, increasing prices and the limited reserves [1], renewable energy has become very attractive solution. Furthermore Wind Energy Conversion Systems (WECS) have been developing at phenomenal rate over the past 20 years [2], this growth rate can mainly be attributed to the advancement of technology across a various range of engineering fields. Figure 1.1 shows the recent cumulative growth of wind turbine installations across several countries. These technologies have greatly reduced the cost of wind power in terms of $/kWh [3] by increasing the energy capture and efficiency of WECS. Renewable energy targets are being pushed onto electricity retailers in order to attain a specific quantity of energy from renewable sources [2]. In order to meet these requirements new and emerging technologies are being applied, however these technologies have their drawbacks which require addressing. The growth of global wind power capacity over the past 20 years has overcome many milestones, however with the increasing size of wind turbines many mechanical and electrical issues have to be considered.

In order to connect to the grid and deliver power to the network, the AC power from

the wind turbine generator must be converted to comply with the grid standards of the end user's country. Currently the Doubly-Fed Induction Generator (DFIG) system is the most adopted technology in the field, this is partly due to it being a proven technology and the cost of rare earth material prices which may make Permanent Magnet Synchronous Machines (PMSM) an unfeasible option in terms of economics. However for off-shore wind turbine where maintenance is more costly due to difficult to reach locations and expensive equipment, there may be an opportunity for the use of direct-drive PMSM with a fully rated converter due to the reduced maintenance requirement with the removal of the mechanical gearbox, which is the component most likely to fail in the WECS [4].

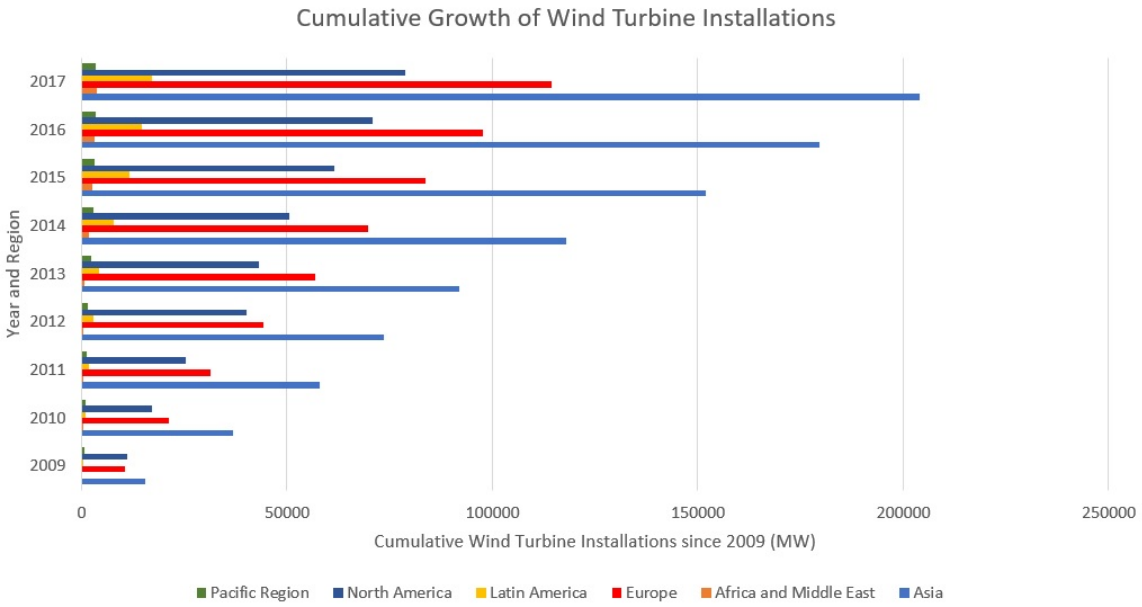

FIGURE 1.1. Wind Turbine Installations. Figure produced from data available from [5].

Typically, the AC power is first converted to DC where the ripple energy is stored in DC link capacitors, it is then converted back to AC at the required frequency and power is transferred to the grid. Currently large wind turbines provide up to 10MW of power [6], these wind turbines require very large capacitor banks in order to reach

required capacitance and voltage ratings, these banks are bulky, expensive and are the least reliable part of the system in terms of electrical components.

This thesis aims to review wind energy conversion systems, in particular large wind turbines employed off-shore where maintenance may be difficult. Furthermore solutions to reduce the maintenance and capacitor requirement are reviewed in this thesis, ideally the solutions would not increase the device count in the converter or the complexity.

Chapter two the literature review reviews possible configurations, topologies and control strategies that may be feasible for the above mentioned objective. Chapter three presents the solution investigated and the validation process of the solution, through simulation and experimental results. The validity of the solution is discussed in the final chapter, and possible further avenues of research are also presented.

CHAPTER 2

LITERATURE REVIEW

2.1 Wind Energy Conversion Systems

Betz' law states that the maximum kinetic energy captured by the wind turbine cannot physically exceed 59.3%. Approximately 45% has been achieved by wind turbines that have been optimized for this purpose [7]. The turbine blades have been engineered to capture wind power at an optimal wind speed, however high wind speeds can cause damage to the wind turbine system. In order to counteract this the most common controls employed are stall control and pitch control [7].

For small-medium sized wind turbines passive stall control is most commonly used, as it is a passive system it is simple and involves designing the turbine blades in such a way that when the wind speeds exceed a specified rate the turbulence generated counteracts the rotational movement of the blade slowing it down. Pitch control is a form of active control that requires sensors, mechanical actuators and controllers, due to the increased cost of the system it is most often used on large wind turbines. The control strategy involves setting the pitch angle of the blades to obtain maximum power capture from the

wind, and when the wind speeds exceeds the rated limit the pitch angle is adjusted to reduce the power capture [8].

The size and capacity of large wind turbines used in wind farms has increased significantly over the past 30 years, ranging from 20m to 162m rotor diameter. With this increase in physical size, the power has increased from 100 kW to 10 MW. This increase in power is due to the relationship between the power captured by the wind turbine and the square of the rotor radius which is equivalent to the rotor area swept (A), shown in equation 2.1. The large wind turbines incur many mechanical challengers such as material stress, however they are offset by the fact the maintenance and installation is much lower than a wind farm capable of producing the same power output formed of many smaller wind turbines.

$$Power = kC_p \frac{1}{2} \rho A V^3 \tag{2.1}$$

The increasing size of wind turbines, and the large quantity required to form a wind farm has become an issue in regards to location. The advantage of having on shore wind farms, is that the maintenance and construction cost is low in comparison with the off-shore farms, additionally they are typically closer to the end user reducing the transmission distance, therefore lowering the associated losses. The wind speed offshore is more predictable and at a higher velocity, this and the issue in regards to visual/noise impact on the environment is one of the main reasons offshore wind turbines are becoming increasingly popular. As wind energy is not a reliable source of power it is most often used in grid connected applications, however sometimes wind turbines are used in conjunction with additional power sources to form a more reliable standalone power source. Most wind turbines generators operate at 690 V, in order to connect to the grid or windfarm substation the voltage is usually stepped up by a transformer to 33 kV.

Figure 2.1 shows a typical wind turbine configuration, where it is interfaced to the

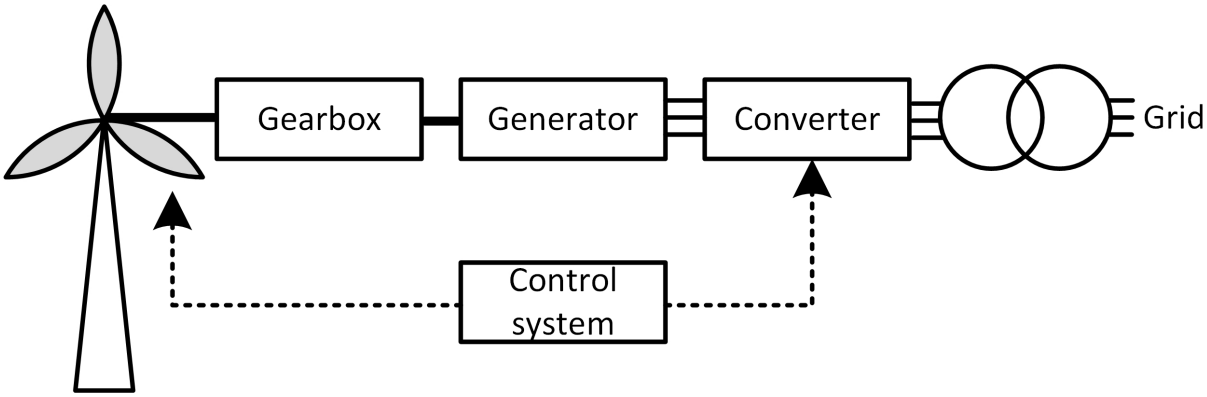

FIGURE 2.1. Wind Energy Conversion System

grid using a converter to ensure it complies with grid codes. Wind turbines rotate at a low frequency due to the wind velocity available and mechanical limitations; although the speed is low the torque is extremely high. As the power is a function of torque and speed, the output power can be in the range of megawatts. As typical a generators rotational speed operates up to two orders of magnitude higher than the wind turbine (1800 RPM for a 4 pole 60Hz machine, approximately 15 RPM for the wind turbine), a gear box is required to match the speed. However if a machine with a large number of poles is used the rotational speed of the generator is reduced, if a significant quantity of poles is designed into the machine the gearbox may be eliminated. Squirrel cage induction generators are most often used in fixed speed wind turbines due to the damping effect on the drive train, removing the need for the generator to be decoupled from the grid. However there is a small range of operational speed of approximately +/-1% of the rated speed, therefore to provide the rated power of the generator a gear box is required to adjust the rotational speed between the turbine and generator. Additionally as induction machines consume reactive power to energize their magnetic circuits, this reactive power may cause self-excitation [9]

Another WECS subcategory is variable speed wind turbines, which uses a converter which is rated to a portion of the full rated generator power output. The advantage

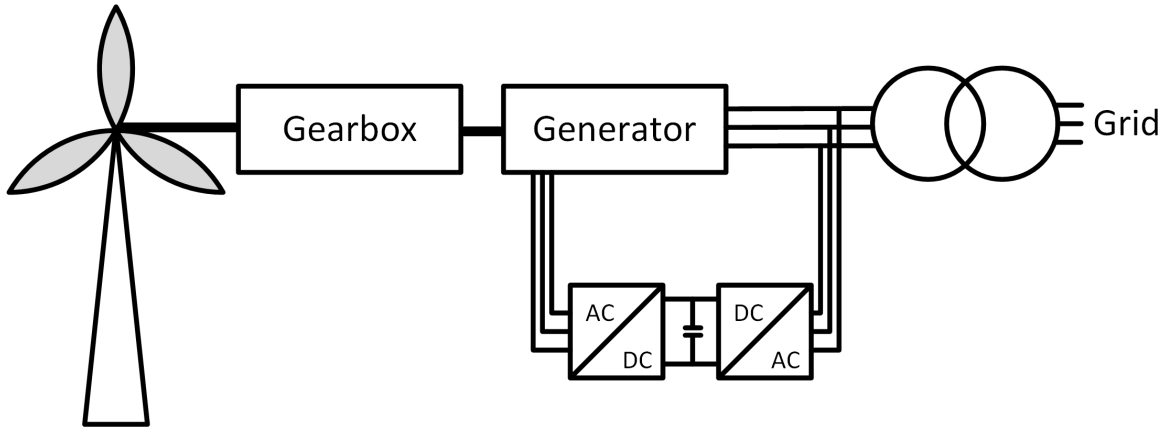

FIGURE 2.2. Doubly-Fed Induction Generator Wind Turbine System

of using variable speed allows for the construction of large wind turbines due to the reduced mechanical stress from smooth operation [10] and there is an improvement on the efficiency of the conversion from the kinetic to electrical energy. Although the cost and complexity of adding a power converter to the system is a drawback, it allows the system to control the reactive and active power delivered to the grid as the generator is de-coupled from the grid [11]. One method to achieve variable speed is to employ a power converter to control the rotor resistance, thereby altering the torque and speed of the generator [12]. Alternatively a doubly fed induction generator can be used to achieve variable speed operation over an even greater range, the power converter is used to connect the rotor of the generator to the grid via a transformer, it is only required to route the slip power. Figure 2.2 shows the typical layout of the DFIG system. As only the slip power is routed through the converter, the losses and cost of the power switching devices are significantly lower in comparison to a converter used for a direct drive system [11].

Some of the key advantages of using variable speed generators is that they are able to reduce the mechanical stresses on the wind turbine structure, this is due to the ability of the system to store energy in the mechanical inertia of the wind turbine which reduces

torque pulsations [13]. Furthermore this contributes to improved power quality as it reduces power variations, and the system may be controlled to dynamically compensate for torque pulsations caused by back pressure of the wind turbine tower [13]. Another great advantage of the variable speed system is that they are cost effective for large wind turbines, this is partly due to the improved system efficiency by having the flexibility to adjust the turbine speed to achieve maximum output power. The technology most adopted for high power wind turbines is the DFIG system, this is in part due to the high cost of rare earth materials making PMSMs expensive and the lower power switching device losses.

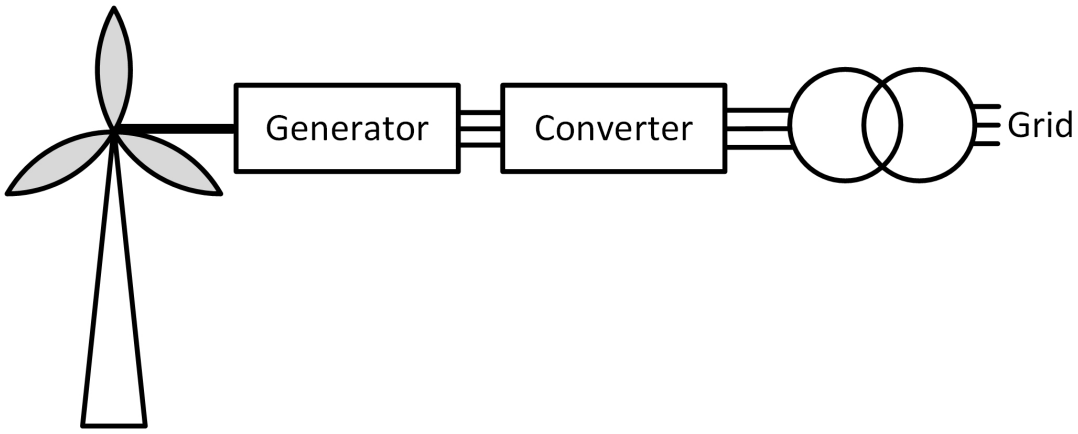

FIGURE 2.3. Direct Drive Wind Turbine System

For off-shore wind turbine applications where the accessibility is an issue and cost and of maintenance is relatively greater than on-shore tubrines, PMSM Direct Drive wind turbines are becoming increasingly popular as they may remove the need for a mechanical gearbox and bearings. Although this increases the reliability of the wind turbine by reducing the complexity and components likely to fail, the direct drive system imposes several new challenges which need to be addressed. As the generator is directly driven by the turbine and rotates at a low frequency (approx. 15 rpm) in comparison to the DFIG system (approx. 1500 rpm), the torque of the generator must increase in order to obtain the same amount of power as the DFIG [14]. For a given flux, a higher number

of pole pairs (P) will give higher torque (T). This is seen in the following equation.

$$T_e = \frac{3P}{2}(\psi_m i_q) \tag{2.2}$$

However the drawbacks of the system are the increased complexity and cost associated with the fully rated converter, in addition to the rotor diameter of the generator due to the number of pole pairs. Recent advancements and cost reductions in the field of power switching devices in addition to the increased up-time of the WECS due to the increased reliability, and the improved efficiency of the system have made direct drive systems a strong candidate for future off-shore wind turbine applications. Figure 2.3 shows the direct drive wind turbine system configuration.

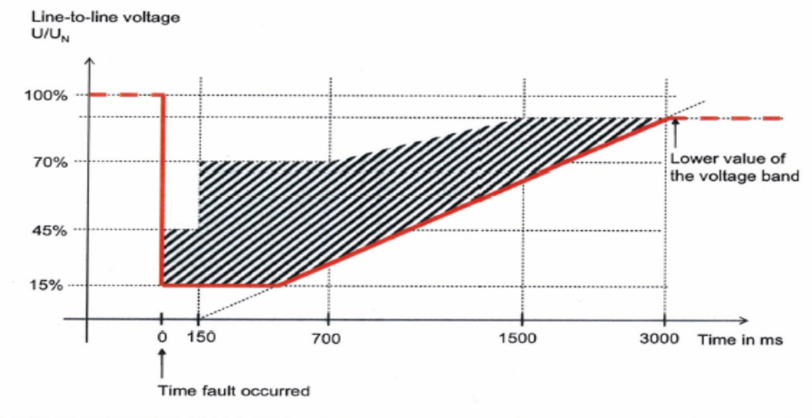

FIGURE 2.4. UK Grid code for Low voltage ride through (LVRT), figure taken from [15]

Table 2.1: IEEE Std 519-1992 Harmonic Voltage Limits

Voltage Distortion Limits		
Bus Voltage at PCC	Individual Voltage Distortion (%)	Total Voltage Distortion THD (%)
Below 69 kV	3.0	5.0
69 kV to 161 kV	1.5	2.5
161 kV and above	1.0	1.5

Table 2.2: IEEE Std 519-1992 Harmonic Current Limits

Current Distortion Limits in Percent of Maximum Load Current at PCC						
% of load current	<11	11≤h<17	17≤h<23	23≤h<35	35≤h	TDD
<20	4.0	2.0	1.5	0.6	0.3	5.0
20<50	7.0	3.5	2.5	1.0	0.5	8.0
50<100	10.0	4.5	4.0	1.5	0.7	12.0
100<1000	12.0	5.5	5.0	2.0	1.0	15.0
>1000	15.0	7.0	6.0	2.5	1.4	20.0
Even harmonics are limited to 25% of the odd harmonics limits						

As the wind turbine market is growing rapidly and the majority of them are connected to the grid, the impact they have on the grid must be considered carefully. As grid codes have been updated to accommodate for the increasing portion of power coming from wind energy [16], wind farms should be able to operate in a similar manner to fossil fuel power plants. The wind energy conversion systems are expected to provide reactive power control, maintain power quality, provide system protection, and regulate the frequency and voltage. Often the main challenge to comply with the grid code is to achieve the fault ride-through requirements, it requires power generating systems to operate continuously even if there is a severe voltage drop for a given amount of time [17]. An example of the UK grid code for wind turbines is shown above in figure 2.4

2.2 Converter Topologies

Power electronic devices have seen rapid advancement in particular the voltage and current handling capability of these devices, additionally alternative materials such as silicon carbide are being developed for use within these devices, and this will increase the power density of the converters allowing for easier integration into wind turbines and a variety of other applications. Power converters can essentially be split into two categories, grid commutated converters and fully controlled converters. The former is

traditionally used in high voltage systems due to the lack of high power devices available with turn off capability, while the latter has found application across a wide variety of applications. However with the advancements in the power electronic devices, IGBTs are rated at 6.5kV and up to 2500A which are being employed for high power applications and can provide full control of reactive and active power as they are fully controlled, conversely control schemes often using pulse width modulation have to be developed which adds to system costs and complexity. Additionally as these converters operate at a high switching frequency they induce harmonics into the system, however these may be filtered out by a small filter [9].

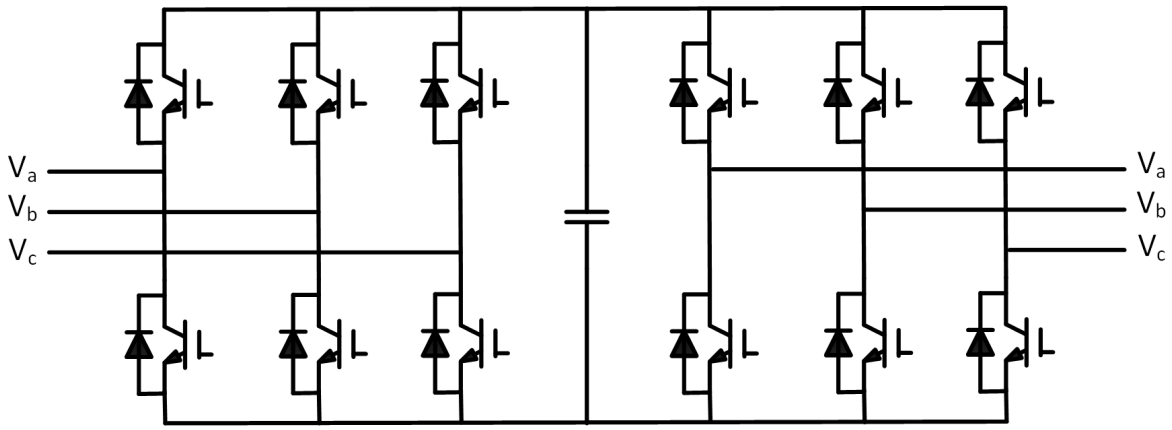

FIGURE 2.5. Back-to-Back Two level 3 Phase Voltage-Source Converter

Currently the most adopted topology in wind turbine systems is the back to back two-level 3-phase voltage source converter (VSC); it can be seen in Figure 2.5, it has been used extensively in other applications and is reliable due to the low device count and robust performance [18]. However a drawback with this topology is that even when using current state of the art power switching devices, you may be required to connect several devices in series or parallel in order to achieve the ratings associated with a large direct-drive wind turbine. This may add to the control complexity of the system as the devices vary slightly due to the nature of the manufacturing process, which may

cause uneven turn-on. Furthermore at higher switching frequencies and voltage levels it may be favourable to employ a 3-level converter, which would also reduce filter size requirements in addition to lower switching losses [19].

2.2.1 Multi-Level Converters

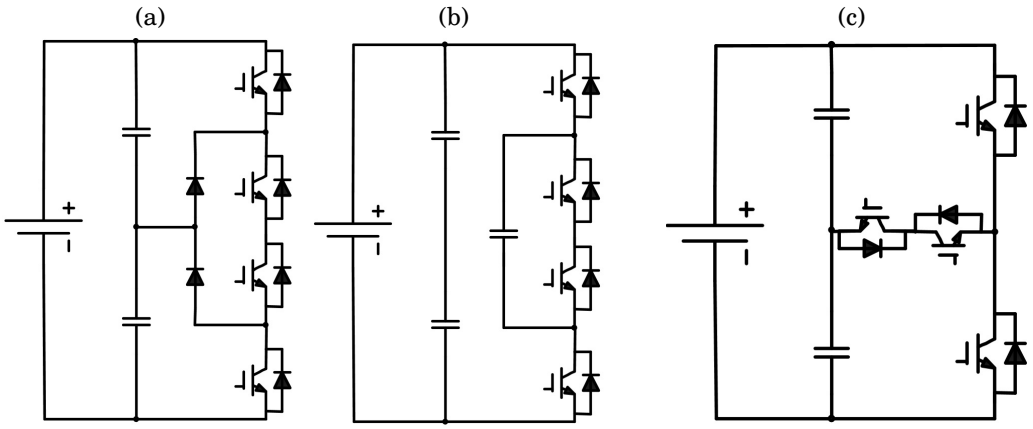

FIGURE 2.6. From left to right, Neutral Point Clamped Converter (a, NPC), Flying Capacitor Converter (b, FCC), T-Type Converter (c)

Table 2.3: Converter Component Comparison

Typical 33kV System using 6.5kV IGBTs			
	3-level NPC	3-level NPC	3-level T-Type
Devices in series	3	3	3
Capacitors per phase	2	3	2
Diodes per phase	2	0	0

One of the issues of using two-level converters in medium-high voltage applications is the harmonics induced by the large voltage step during the switching process and high switching frequency, one solution to reduce the harmonics is to use multilevel converters. These converters have already been successfully used in industry, and are gaining increasing popularity as the solution for high power electrical conversion [20]. Although the concept and application of multilevel converters is not new, the complexity

of the converters pose additionally challenges which open the door for plenty of research opportunities. The advantage of using multilevel converters is that readily available and reliable power switching devices may be used to achieve high electrical power conversion; however the circuits are more difficult to implement and require more advanced control solutions. However in retrospect the use of traditional 2 level voltage source converters and current source converters (CSC) are not always feasible for high power applications due to the increased requirements of the filter design.

The key advantages of using multilevel converters is that the voltage is split across the devices allowing the system to handle higher voltages, due to this the voltage derivative is also reduced along with the common mode voltages. The output waveforms of the current are near sinusoidal, this may allow for the input and output filters to be removed or reduced. Additionally when operating at high switching frequencies they are more efficient than the 2 level converters. Some multilevel topologies provide a modular design, which can allow for fault tolerant operation which is an increasingly popular feature in order to maintain power and power quality. It is because of these reasons that they have found application in industry in a variety of fields such as pumps, fans, traction drives [20], they have also found application in hybrid/electric vehicles and renewable energy solutions.

The number of voltage steps that can be produced by the converter is what defines how many levels a converter is able to generate, the more levels the smoother the output waveform and the harmonics are also reduced. The levels are usually produced by adding addition capacitors, diodes and switches. For two level converters adopting pulse width modulation control schemes, the voltage amplitude and frequency are both controllable [21], by using multilevel converters the additional voltage step allows for additional alternatives to synthesize the waveform.

There are a wide variety of topologies that are able to generate multilevel voltage

waveforms, each design has advantages and disadvantages however some have not found application in industry due to the complexity of the circuit and control scheme, or because of the risks associated with adopting an unproven technology. One of the most common multilevel topologies found today is the flying capacitor converter, seen in Fig 2.6b. It was introduced in 1992 and uses a single DC source to generate the multiple levels [22]; it is also referred to as a multi-cell converter as it can be stacked to become modular and can continue to function when a power cell is not operational. The flying capacitor topology is very similar to the Neutral point clamped (NPC) topology (also seen in Fig 2.6a), the main difference is the clamping diodes are interchanged with capacitors.

The three level neutral point clamped converter is similar to the standard two level voltage source converter in terms of schematics; essentially it is two of the converters stacked upon each other with the addition of clamping diodes to form the neutral point which provides the third voltage level. As the devices only see half of the DC link voltage [23], the semiconductor power devices may be scaled down or the power rating of the converter may be increased. However as there is only one switching combination that generates the zero voltage level, there is less freedom for the control scheme to distribute the losses evenly, therefore the outer upper and lower devices incur significantly more losses than the other power switching devices which poses a limitation in terms of increasing the power handling capability or switching frequency of the converter. This converter is not typically used for applications requiring a high number of levels and high power; this is due to the requirement of the clamping diodes being able to block high voltages. The same limitation applies to the FCC due to the complexity control strategy required to balance the DC-link capacitor.

As mentioned above one of the drawbacks of the NPC converter is the uneven loss distribution between the inner and outer power switching devices, one solution to this is to interchange the clamping diodes with an active bi-directional switch which prevents

the current freewheeling through the diode and adds another degree of control freedom [24]. The ability to generate the zero voltage level using two different combinations of switches [20], is what gives this control freedom, which allows the power losses to be distributed across the devices more evenly when an appropriate control scheme is applied in comparison to the NPC converter. With the active switches the current flowing through the neutral point can be controlled to flow through the upper or lower path allowing for a more even distribution of semiconductor losses. This is known as the neutral point piloted (NPP) converter, it is also known as the T type converter (seen in Fig 2.6c), it has been gaining increasing popularity as it connects IGBTs in series to lower the switching losses [25]. Essentially the T-type converter benefits from the low conduction losses associated with the two level voltage source converters, and the lower switching losses of the NPC converter. The series connection of the devices reduces the current passing through them by a factor of two; this allows the switching frequency to be doubled. The output voltage waveform and PWM control strategy is the same as the one used for the NPC converter. The overall loss for the system for the system in comparison to the NPC converter is the same; however the losses are more evenly distributed for the NPP converter. For medium voltage drives the application of three-level converters is ideally suited to power ranges from 300 kVA - 30 MVA [26], Seimens have developed commericial drives up to 24 MVA incorperating 3-level converters [27].

These multi-level converters may be scaled up further to provide increased voltage steps, however few of these topologies have found their way into real world applications due to complexity and control issues, in addition to more established topologies being favoured by end-users due to reliability. By employing multi-level converters on the grid-side converter of the WECS, it may be possible to achieve connection to the grid without any passive filters [28] due to harmonic reduction, this may reduce the cost and losses of the overall system. One of the key issues with increasing the number of voltage

levels in the above mentioned converters is that large quantities auxiliary components are required, such as flying capacitors and clamping diodes. These components add to the control complexity of the converter, and special consideration is required when developing PWM and control strategies to ensure voltage is balanced across the capacitors [29][30].

2.2.2 Full-Bridge Converter

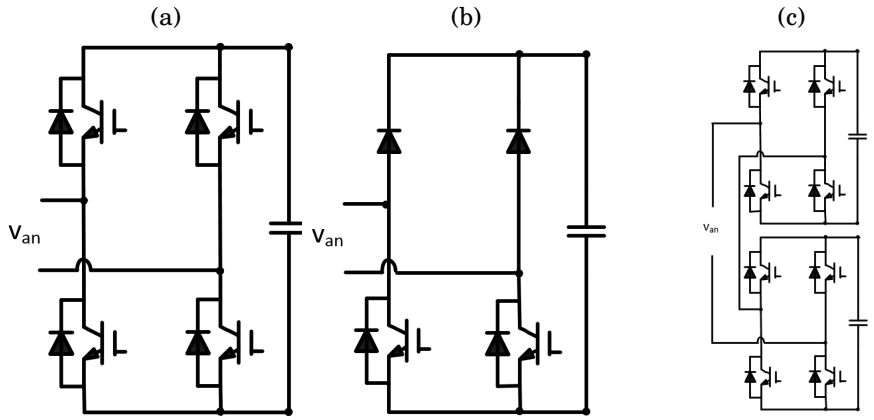

FIGURE 2.7. From left to right, Full-Bridge (a), Semi-Bridge (b), Cascaded-H-Bridge (c)

A simple diode bridge with an output filter capacitor only allows the DC voltage to track the peak of the AC input voltage; this also produces a lot of distortion on AC input current. The benefits of using a full bridge (seen in Fig 2.7a) topology is that the input current harmonics are reduced, improved power factor operation and bidirectional power flow [31]. The full bridge converter, commonly referred to as the H-bridge converter consists of a pair of two-level VSC phase legs. The full bridge is able to produce a three level voltage output waveform as the output of the converter is the line to line voltage between the two phase legs [20]. The cascaded H-bridge converter is able to produce the highest number of levels for the fewest switching devices. The multilevel output of the cascaded H-bridge is generated by connecting the converters in series;

the combination of the outputs can be used to synthesize the required waveform. Each H-bridge is modular, if a bypass switch is added the converter can continue to operate even when one is the bridges is not functioning due to the redundancies, additionally the output voltage and rated power of the converter is increased by connecting additional modules. A key advantage of this topology over the FCC and NPC converters is that there is no requirement for clamping diodes or flying capacitors, in addition to having a relatively simple structure and control technique [32].

To achieve higher voltage handling capabilities devices may be connected in series like traditional medium-voltage drives, however it is favourable to connect the H-bridge topology in series rather than the individual devices. This structure is known as the Cascaded H-Bridge, the advantage of this topology is the ability to generate multiple levels depending on the number of H-bridge connected in series. Furthermore the cascaded H-bridge is a modular structure which makes it ideally suited for off-shore applications as it is an inherent fault tolerant structure. In a typical VSC when a single device fails, the entire converter cannot continue operation. However with the suggested topology if a single device fails, the cell that contains that device may be bypassed with a switch and control scheme which will allow the converter to continue transferring power to the grid and at a lower power or voltage output. Traditionally redundancy has been achieved in the 2-level VSC by connecting twice the required press-pack IGBTs in series; which fail as a short circuit, allowing the system to continue operating at the rated voltage and current. Although the reliability of the system is increased, the device count is also doubled, introducing more complexity and costs. The cascaded H-Bridge having an inherent modular structure, capable of providing redundancy makes it a strong candidate for off-shore applications [33].

One of the main drawbacks of this topology is the requirement for an isolated DC source for each bridge, however by using DC sources carefully selected according to

the required number of levels at the output, the redundant switching states may be eliminated and additional levels may be generated, this is also known as the asymmetric cascaded converter. Conversely this will produce a lower output voltage in comparison to using the same power switching devices to produce a smaller quantity of levels [34]. When using this topology with a DC-source, as would the case in a back to back configuration capacitor balancing issues are minimised as they may be handled by the opposing converters control strategy. One of the key advantages of using a modular topology is the ability to connect the converter modules in series, which each module increasing the voltage handling capability of the system. Furthermore it may be possible to reduce the voltage rating of the devices selected for the application, in comparison to a typical VSC this may reduce the cost of the total devices [35].

When considering this topology for direct drive WECS due to the low frequency output of the generator and the voltage ripple across the DC-Link; being equivalent to twice the generator frequency, the capacitor bank will be extremely large. Furthermore in order to achieve the required capacitance and voltage ratings electrolytic capacitors may have to be used, this will reduce the reliability and lifetime of the WECS. When considering off-shore applications the costs of maintenance can be great, therefore being able to improve the reliability or reduce/remove the capacitor requirement could reduce the unit cost of wind generated power.

Back to back converters are required in variable speed wind turbines that employ a full scale power converter. These converters are either unidirectional or bidirectional allowing power flow in both directions. The bidirectional converter requires a switch that can pass current in either direction, this is usually done with a semiconductor switching device such as an IGBT, with an anti-parallel diode, the advantages of using a bidirectional back to back converter in comparison to a diode rectifier is that the system is able to more reliably able to reach reactive power requirements, additionally it is able

to provide better power quality on the stator side. Furthermore a full scale converter is able to maintain the low voltage ride through requirements of the grid code [36]. However the addition of fully controlled power switching devices adds to the cost and complexity of the system, due to this unidirectional systems are an attractive solution where the power factor requirement is close to unity [37]. For large permanent magnet synchronous generators used in wind turbines where the phase difference between the voltage and current is relatively small the unidirectional converter may be applied, this will still maintain the minimum generator size during the design process but with the benefit of having fewer controlled power switching devices reducing systems costs and control requirements. The grid side converter's control scheme may account for the Low Voltage Ride Through (LVRT) requirements of the grid [38].

2.2.3 Semi-Bridge Converter

One solution to reducing the semiconductor costs of the full bridge is to replace the upper power switching devices with diodes, this is known as a semi-bridge or bridgeless PFC converter. By using the semi-bridge the problems associated with shoot-through are alleviated and the quantity of controlled power switching devices is reduced. The converter also maintains some of the benefits of using the full-bridge topology such as reduced harmonics, dc-link voltage fluctuations and simplified transformer design [39]. The semi-bridge is a uni-directional converter, as it unable to provide a path for the current to flow when the voltage and current are of opposing polarities; this constraint means that there is no reverse power flow or conduction, this reduces the converters ability to maintain a sinusoidal current through a range of power factors[31].The topology can be seen in 2.7b.

The semi-bridge can be operated with a variety of different control algorithms, including bi/uni-polar PWM switching designed for H-bridges however the system will

not be able to operate in all four quadrants like the full-bridge. A popular method to control the converter is average current control, where the inner current loop is used to regulate the inductor current and the outer voltage loop usually used to regulate the DC-Link voltage is multiplied by the phase of the input voltage. Another popular control algorithm is One Cycle Control, as the bridge-less boost converter is essentially two boost converters it is possible to calculate the duty cycle according to the input voltage and inductor peak current [40]. Another advantage of the converter is the lower device count in the current conduction path, reducing semiconductor losses when compared to a typical PFC boost rectifier[41]. This topology may also be cascaded in a similar manner to that of the full-bridge converter, if a few cells are interchanged with H-bridge cells the converter may have improved an input current waveform when operating at non-unity power factors.

2.2.4 Matrix Converter

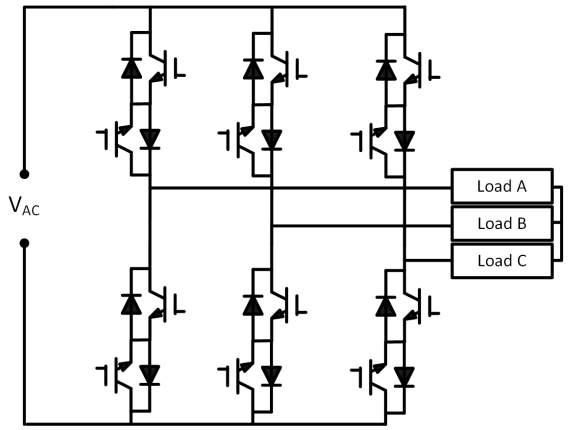

FIGURE 2.8. Single Phase to Three Phase Matrix Converter

Another solution to reducing or removing the DC link capacitor is to use the matrix converter (shown in figure 2.8; there are a variety of potential benefits to be gained by using this technology. In comparison to a typical AC-DC-AC converter, the conduction

losses may be lowered as reverse blocking devices may be used, this reduces the number of devices in the conduction path [42], however this may be offset by the increased voltage drop of these devices due to the manufacturing processes required to create the reverse blocking feature. As the matrix converter is bidirectional it is able to control the power factor of the generator allowing for improved efficiency and reduced size. One of the key advantages of the matrix converter is that the requirement for a DC link capacitor to absorb the pulsating power is removed in principle, this increases the reliability of the system greatly and makes this an attractive solution for off-shore wind farms. However the control of the matrix converter is more difficult than the conventional DC link converter, this is due to the current commutation paths required. The requirement is that there must always be a path for current to flow out of each phase leg of the converter, however if both switches are closed at the same time shoot through will occur and if both switches are open large transient voltages are experiences by the system and will cause device breakdown [43].

2.3 Control systems

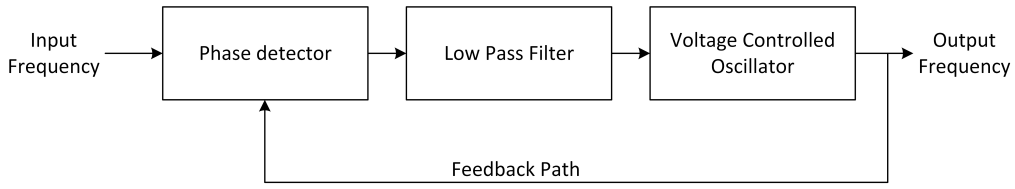

FIGURE 2.9. Phase Locked Loop Control Schematic

When designing a control system for a WECS to connect to a strong grid such as the UK, the generator side converter is used to perform maximum power point tracking (MPPT) [44], this also determines how much power is transferred to the electrical network. The grid side converter is used to control the DC-link bus voltage of the converter, during normal operation and grid faults. In order for the system to track

the phase of the grid current; which it will be interfaced with (hence the name grid-tie inverter), a phase locked loop (PLL) is typically used (the control structure is shown in figure 2.9). The PLL is used to determine the network frequency and phase [45].

PI controllers require tuning in order to operate in the required manner for a given system. There are a variety of different tuning methods and theories that have been developed, each focusing on the settling time, overshoot of the system, however these tuning methods are based upon a model of the system which is often only a rough representation[46]. This can cause unexpected responses from the control system; therefore it is often important to manually fine tune the controller. Module optimum tuning method requires a model of the system in the form of an open loop transfer function; the PI controller is used to cancel the slowest pole resulting in a control system that is stable and has optimum rise time when considering overshoot.

As mentioned previously the PI controller is only able to operate at DC and very low frequency, this is due to the gain of the controller being relatively high in that range. Many methods to increase the bandwidth of these controllers have been proposed in literature, however these methods often cause the system to operate very close to the stability limits, these methods include adding a grid voltage feed forward path, increasing the proportional gain of the controller and multiple state feedback. These methods also help to overcome some of the short comings of the PI controller such as the AC steady state error/tracking [47].

2.3.1 Generator Control Schemes

Field orientation control is the most common type of control implemented in wind energy conversion systems and AC drives [48]. This control strategy involves decoupling the control of the electromagnetic torque and rotor flux, it is imperative that the rotor flux orientation is known to a high degree of accuracy. By using the rotor flux orientation the

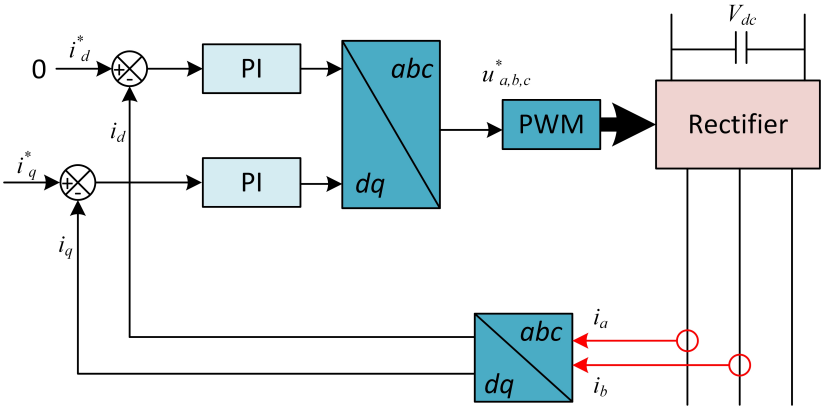

FIGURE 2.10. ZDC Control Schematic

generator's stator current can be decomposed into the torque and flux components which are then controlled individually to achieve high dynamic performance.

A more advanced control strategy is direct torque control (DTC), the advantage of this control scheme is that it is much simpler and does not require coordinate transforms reducing computation burden, additionally it does not need current regulation. This is achieved by comparing the reference values of the torque and flux with the estimated values, the difference is the error and this can be used to regulate the converter states in order to reduce the error to a predefined range [49]. However due to the simplicity of the control scheme, it requires relatively high frequency to obtain good torque control, for this reason high torque and current ripple can be seen especially at low frequency.

Zero d-axis current control is as the name suggests, by setting the d-axis current to zero the relationship between the electromagnetic torque and stator current becomes linear. In order to do this the three phase stator currents must be transformed from the stationary reference frame to the synchronous reference frame (d and q axis components). As the d axis current is set to zero, the stator current is equal to the q axis component. Assuming the rotor flux linkage remains constant, the torque has a linear relationship with the stator current [50].

Maximum torque per ampere control uses the minimum stator current to generate

the required amount of torque. This is based on the on the fact different values of stator currents in the synchronous reference frame are able to produce the same value of torque. The control scheme adjusts the ratio between the d and q axis components to produce the maximum torque per ampere. In a non-salient machine the d and q axis inductances are identical therefore by setting the generators flux producing current to zero (the d axis component), the torque is generated with the minimum stator current as it will be directly equal to the q axis component [50]. An example of zero d-axis control scheme is shown in figure 2.10.

2.3.2 Auxillary circuit DC-Link reduction

One method to reduce the DC-Link voltage ripple is proposed in [51][52], an active power decoupling circuit is designed with energy storage elements and a bi-directional buck-boost converter. The pulsating power generated by the PFC bridgeless converter is transferred to the auxiliary energy storage elements, and released back to the DC-Link through the bi-directional converter. This occurs twice per fundamental cycle, as the DC-Link frequency is at twice the fundamental.

2.3.3 Resonant Controller

The conventional proportional-integral (PI) control has been studied extensively in literature and found a wide variety of applications in industry. It is able to provide a high gain at DC, therefore when adopting this controller for a AC system it is required that you perform the park transformation in order obtain the dq values of the system. In order to overcome this issue it may be feasible to use the resonant controller as it able to provide a high gain at a selected frequency, essentially it operates as a notch filter. The differences between the two controllers can be seen in figure 2.11. Due to the infinite gain at the resonant frequency, the controller should be able to track an AC signal without any

steady state errors [53]. Due to the characteristics of the controller it has found several applications such as selective harmonic reduction, where multiple resonant controllers are set to operate at frequencies where harmonics are generated, and the controller is able to filter them out [54][55]. It has also found application in reducing torque and current ripple in traction drives [53], by compensating for the DC-Link ripple power generated by the rectifier.

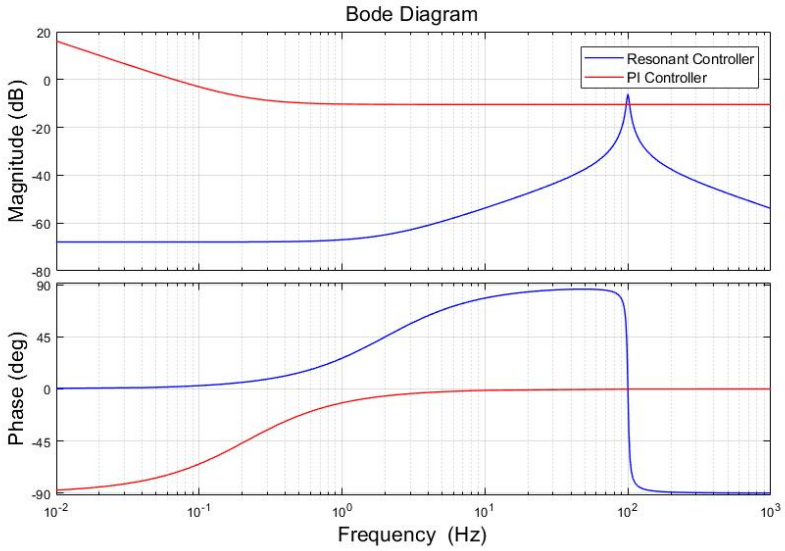

FIGURE 2.11. PI and Resonant Controller Bode Plot

2.3.4 Non-ideal resonant controller

The function of the resonant controller is to produce an infinite gain at a selected frequency known as the resonant frequency; this eliminates the steady state error in a similar manner to the integral controller used to reduce the DC steady state error. However the problem with having an infinite gain is that the system can induce resonance and cause the system to become unstable, this can cause undesirable results. One solution to this is to use the quasi-resonant controller; the controller has a finite gain that is still able to attenuate a small steady state error, also the bandwidth may be

increased to reduce sensitivity to variations caused by sensing equipment, grid frequency variation and noise. The implementation of these controllers may be done using an analogue approach, however digital implementation is often preferred due to ease of modification. However digital implementation requires discretisation which has on the zeros of the system, this can cause instability issues depending on the distribution of the zeroes in regards to the continuous transfer function [56].

2.4 Summary

As this thesis focuses on large wind turbines, the direct drive variation of the wind energy conversion system is attractive. Employing a PMSG with multiple poles to match the generator speed may be feasible and will be investigated further. Due to the large DC-Link voltage ripple caused by low frequency of turbine and generator, it may be beneficial to employ a method to combat this. An Auxiliary circuit would require addition components and bring more complexity and possibly a higher chance of failure, therefore the resonant controller will be further investigated as it does not increase the device count. However the resonant controller has its own drawbacks which are discussed in the next chapter.

CHAPTER 3

DC-LINK VOLTAGE RIPPLE REDUCTION METHOD

3.1 DC-Link voltage ripple reduction method

In order for a wind energy conversion system using a synchronous generator to connect to the grid, a fully rated power converter is required. When using a machine with a large number of poles, the gearbox requirement is removed, however output frequency of the waveform produced by the generator is very low, this coupled with the fact the wind turbine employing this type of machine will typically be designed to produce high power (in the range of 1.5 MW to 10 MW) poses an issue on the energy storage elements of the circuit, the DC link capacitor. Due to the relationship between the power, frequency and capacitance the size requirement of the DC link capacitor increases greatly. One of the main issues with the large capacitance requirement at a high rated voltage is that electrolytic capacitors must be used. Electrolytic capacitors are the most unreliable part of a wind energy conversion system that does not use a gear box; this poses a reliability issue which is an important factor for offshore windfarms [57]. If the DC link capacitor can be reduced or removed, the system will be more reliable and may require

less frequent maintenance. The cascaded H-bridge produces pulsating power at twice the generators supply frequency, the traditional proportional integral (PI) controllers are only able to control DC values, the implementation of the resonant controller which is also known as an idealized AC integrator allows for the pulsating power to be attenuated, this is used to actively control the three phase voltage source converters connected to the H-bridge. One issue with the implementation of the resonant controller is that the current on the converter side is not sinusoidal and this has adverse effects on transformer losses, and the thermal cycling of the IGBT which may reduce the lifetime of the power switching devices [57]. However, this does not affect the quality of the power delivered to the grid, as the harmonics are negated in the transformers secondary windings.

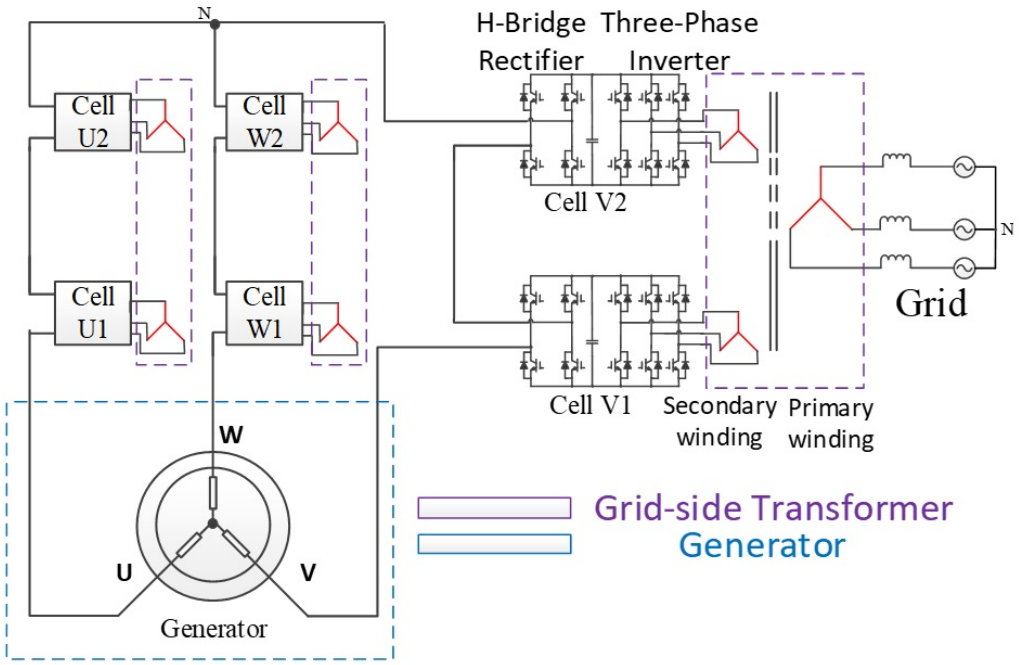

FIGURE 3.1. Large Wind Turbine Converter System

A set of multi-level modular medium-voltage high power converter for wind turbines have been developed in [58], and experimental results for a single cell have been presented in [57]. These have been thoroughly analysed and results have been recreated in order to develop the system further. Fig. 3.1 shows the suggested topology, where each

cell consists of a H-Bridge converter used to rectify the current supplied by the PMG and perform maximum power point tracking (MPPT). As the stator frequency is relatively low (5 to 15 Hz), this rectification process generates a large voltage ripple across the DC-Link capacitor. The issue with using electrolytic capacitors as mentioned previously is the reliability of the component, and when considering off-shore applications the costs of maintenance can be great.

A two-level voltage source converter is used as a grid tie inverter in each cell, it is actively controlled using the resonant controller in addition to the standard PI control. The controller is set to have a resonant frequency at the same frequency of the ripple present on the DC-Link, this allows the inverter to compensate the pulsating power by transferring it across the DC-Link and may remove the need for storage elements. Ideally the grid side isolation transformer is placed outside the nacelle at the bottom of the wind turbine structure; this reduces the mechanical stress on the tower, which has become an important consideration when looking to enter into the 10-20 MW range of wind turbines. This has been made possible due to the reduced current rating when using multi-level topologies, as the I2R losses of the cables running down the tower to the transformer are reduced greatly. However the insulation rating of the cables, and switch gear will need to be increased, in order to contain the higher voltages the system is operating at. In addition to providing isolation the transformer also steps up the voltage from the converter up to the grid voltage.

The cascaded H-Bridge topology has been applied successfully in medium voltage motor drives, ranging from medium to high power in industry and research areas. It may become a strong candidate for future large wind turbines.

3.1.1 Control

The generator is modelled in the synchronous reference frame. As a synchronous non-salient permanent magnet is analysed in this paper for this application, zero d-axis control (ZDC) is implemented which also performs maximum torque per ampere (MTPA) control. The converter achieves MPPT by adjusting the generator speed according to the wind speed, using a reference table with pre-determined values according to the generator characteristics, a PI regulator is used maintain the reference values. The cascaded H-bridge is modulated using phase shifted pulse width modulation (PS-PWM), which is implemented using a time delay on the consequent bridges connected in series, the value of the time delay is adjusted according to the number of cells. For a direct drive large wind turbine and the proposed topology, a large DC link capacitor is required in each cell in order to reduce the voltage ripple; despite the fact the H-bridge produces a ripple at twice the fundamental frequency. This is due to the high power rating of the wind turbine, the generator stator frequency being a relatively low value, and the benefits of keeping the capacitor ripple as low as possible. The effects on the voltage ripple can be seen in the following equation, where ***Vr*** is the rectified voltage.

$$\Delta V = \frac{P}{2\pi f \cdot C \cdot V_r} \tag{3.1}$$

By reducing the ripple seen on the DC link, the capacitor may operate at a lower temperature as it must store less energy; this may increase the lifetime of the capacitor. This would reduce the requirement for maintenance, which is a huge factor for large off-shore wind turbines as there are large costs associated. Typically for a large converter system, the DC-link capacitor bank occupies a third of total volume. In order to reduce the size of the DC link capacitor, the control scheme shown in Fig. 3.2 has been implemented to control the grid side three-phase inverter. Where the system employs dq control, and the DC reference value is maintained by the proportional-integral controller, additionally

a resonant controller has been implemented to actively control the grid side inverter to attenuate the DC link voltage ripple generated by the H-bridge in each cell.

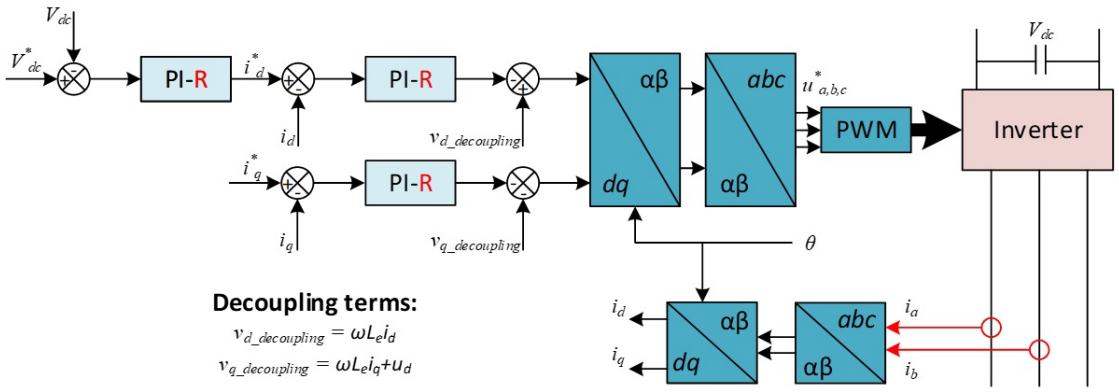

FIGURE 3.2. Grid-Side Converter Control

The grid voltage is aligned to the d-axis in the synchronous reference frame, where the amplitude is equal to the transformers secondary winding voltage vector. This allows the converter to actively control the active and reactive power independently using d and q respectively. As shown in Fig. 3.2 the outer voltage control loop provides the current reference for the d-axis control loop. Both inner current control loops are set to operate at a rate 10 times faster than the voltage control loop. The q-axis is typically regulated to be zero, in order to provide unity power factor operation.

The PI controller is tuned using the pole zero cancellation method, as the inductance and resistance values of the system are known (1mH and 0.01 Ohms respectively). The current loop bandwidth is set to be 300Hz, a sixth of the switching frequency. Using the values described, the coefficients for the PI controller can be calculated, where $K_p = L * \omega_c$ and $K_i = R * \omega_c$.

One of the issues with this topology when applied to motor drives is the additional harmonics present in the current, due to the use of a diode rectifier. These harmonics are reduced by using a multiple winding phase-shifted transformer, however as the grid

side inverter is actively controlled it may remove the harmonics without the need for a specific transformer for this purpose. Furthermore the transformer leakage inductance may be used as filter inductance, possibly removing the requirement for an additional AC choke, if the transformer is large enough.

With the control active there are several drawbacks which are discussed in [58], the cause of these drawbacks is due to the harmonics induced into the current waveform with the control active. These harmonics are present in the transformer secondary windings due to the attenuation of the single-phase pulsating power generated by the H-bridge, additionally through analytical analysis shows the transformer incurs additional 50% copper losses, which should be considered during the design phase [58]. Another consideration is the harmonics present in the current waveform may put the power switching devices through harsher thermal cycling conditions, when compared to the conventional PI control; this may reduce the lifetime of the devices and therefore increase the maintenance costs.

However for a three-phase wind turbine system, the grid side power quality may not be affected, as the power delivered by a three-phase system is constant and the harmonics should annul each other out in the transformer windings, and produce a sinusoidal current on the primary side.

3.1.2 Simulation Results

Table 3.1: Simulation Parameters

Wind Energy Conversion System Simulation	
Paramter	Value
Power Rating (MW)	10.0
Substation Voltage (kV)	33
DC-Link Voltage (V)	1800
DC-Link Capacitance (mF)	50
Cells per phase	5

With the simulation file provided for a large wind turbine system providing 10 MW, the effects of the resonant controller can be observed. Figure 3.3 shows the DC-Link voltage ripple and the resonant controller is active after 2 seconds, the affects of the compensating for the ripple power that was previously present on the DC-Link is now seen in the transformers secondary windings (seen in Fig 3.4). This may cause additional device stress and losses, however as discussed in [58] the harmonics generated by the pulsating power in the three-phase system cancel each other out, therefore a sinusoidal waveform is seen at the primary side (seen in Fig 3.4).

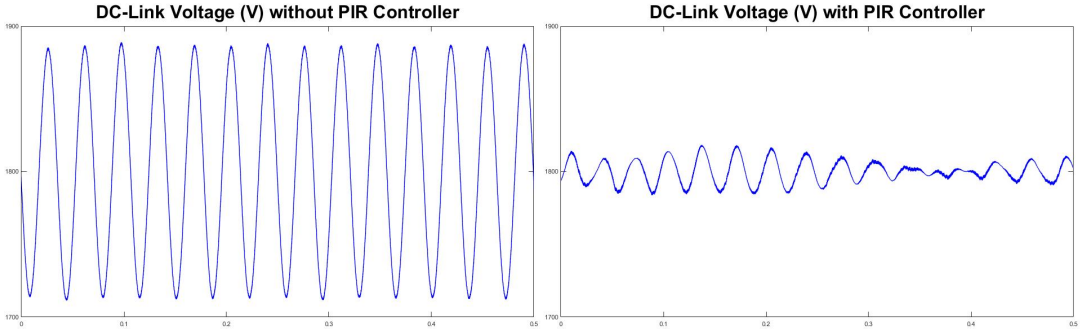

FIGURE 3.3. DC-Link Voltage Ripple

3.1.3 Single Cell Experimental Results

Single cell experimental results have been presented in [57], one of the key issues found during the experimental process is that the resonant frequency is very sensitive to slight shifts in the fundamental frequency. Therefore the resonant frequency would require manually adjustment in small increments until the controller effectively attenuated the DC-Link ripple, however this method is not very robust. The previously mentioned issues were present when using the grid to emulate a generator output, and feed the converter power which is then transfered back to the grid through the multi-winding transformer. The grid has a relatively stable frequency, this issues may be exaggerated

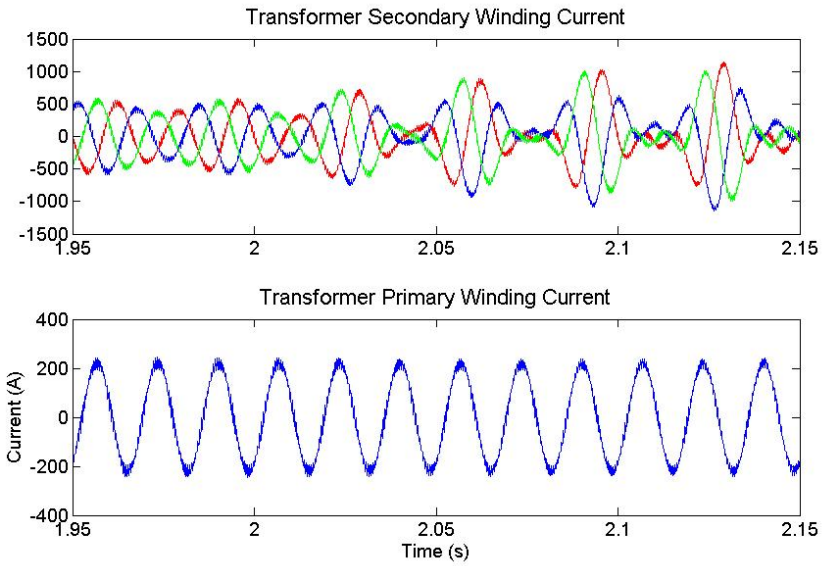

FIGURE 3.4. Transformer Winding Current

in a WECS (where the frequency would vary depending on the wind speed); therefore the quasi-resonant controller has been suggested to overcome these issues.

3.2 Implementing quasi-resonant controller

The quasi-resonant controller has an additional control variable, in comparison to the standard resonant controller; this variable wc increases the bandwidth of the controller, additionally this removes the issue of having an infinite gain with the resonant controller which can cause stability issues and incur resonance in the system. However increasing the bandwidth has adverse effects on the performance of the controller, as the peak gain at the centre frequency (ω) is reduced. Additionally the gain of the controller at all other frequencies in increased, which may have unpredictable results when operating in a non-simulated environment. The ability to provide a large gain at a range of frequencies may allow the control system to operate more reliably in a real world scenario, where the sensing equipment and noise may cause discrepancies [59]. Furthermore as the generator

speed will dynamically adjust according to the wind speed; the DC-link ripple frequency will also change, the quasi-ideal resonant controller may provide better performance as it provides some leniency for the delay of the measured rotational speed [60].

The difference between the two controllers can be seen in Fig 3.5, and the following equations.

Resonant Controller:

$$G(s) = \frac{s}{s^2 + w^2} \tag{3.2}$$

Quasi-Resonant Controller:

$$G(s) = \frac{w_c s + w_c^2}{s^2 + 2w_c^2 s + (w_c^2 + w^2)} \tag{3.3}$$

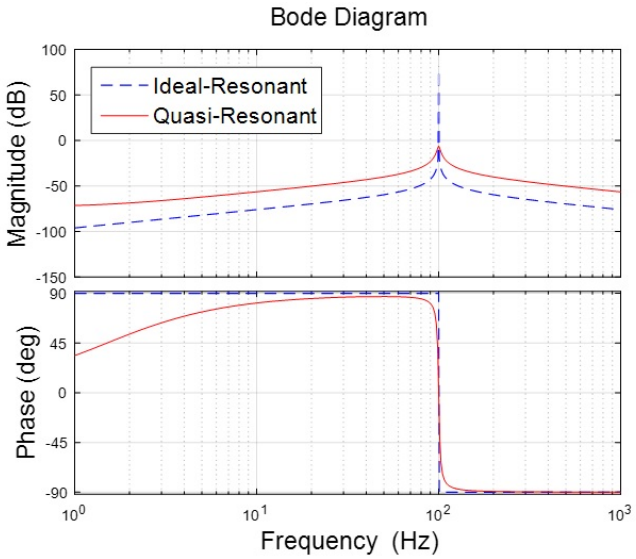

FIGURE 3.5. Comparison of Resonant Controllers Bode Plot

In order to derive the quasi-resonant controller, the simplified form of the quasi-controller is used shown in the following equation:

$$G(s) = \frac{2w_c s}{s^2 + 2w_c^2 s + w^2} \tag{3.4}$$

Another issue faced when implementing the quasi-resonant controller in a DSP, was the limited decimal precision of the fixed point DSP used (TMS320F2812). To overcome this the IQ math library was used which allows the floating point algorithms to be implemented into a fixed point processor.

3.2.1 Simulation Results

In order to implement the quasi-resonant controller on a digital platform the transfer function must first be discretized into the z-domain. The methods of discretization investigated are Impulse Invariance, and Bilinear transform (Tustin). The bode plots for each of the transformations is shown in Fig 3.6. In order to derive the quasi-resonant controller in the z-domain, the simplified form of the controller is used. When discretising it can be seen that the it forms the same structure as a second order filter, therefore the controller can be mapped into bi-quad filter. The second order filter equation is shown in the following equation:

$$H(z) = \frac{b_0 + b_1 z^{-}1 + b_2 z^{-}1}{a_0 + a_1 z^{-}1 + a_2 z^{-}1}$$

If the controller will be implemented into a fixed-point digital signal processor (DSP), it is good practice to multiply through the equation by 1/a0, as this may reduce the decimal precision required for optimal performance of the controller. Additionally this allows us to remove one multiplier from the implementation process, which will reduce computational burden.

The coefficients derived using the Impulse Invariance transform are given in [59], and are as follows:

$$a_0 = 1$$

$$a_1 = -2e^{-2w_c T} cos(wT)$$

$$a_2 = e^{-2w_c T} \tag{3.5}$$

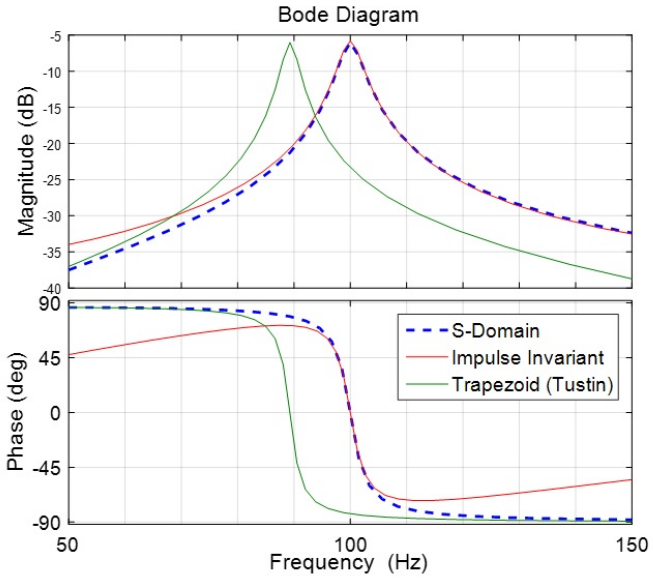

FIGURE 3.6. Comparison of Discretisation Bode Plot

$$b_0 = 0$$

$$b_1 = w_c + we^{-w_c T} sin(wT) - w_c e^{w_c T} cos(wT)$$

$$b_2 = w_c e^{-2w_c T} - w_c e^{w_c T} cos(wT) - we^{-w_c T} sin(wT)$$

The direct form I implementation of the digital bi-quad filter is ideally suited to a DSP, due to the difference equations containing 3 small additions (seen in Fig. 3.7), whereas the direct form II is better suited to a FPGA where there are 2 large additions also shown in Fig 3.7. Additionally if using a fixed point processor it may be preferable to use the transposed form of the filter, as it is not as susceptible to precision issues.

The simulation is based on a 10 MW wind turbine system as described previously and in [58]. The H-Bridge is modulated using a unipolar switching scheme to emulate a three-level phase voltage waveform on the generator windings. When cascading the H-bridges by connecting them in series, the consequent bridges' PWM signals have a phase shift, which is implemented through a time delay. The following equation shows the method of calculation for the degree of phase shift, where N is the total number of bridges connected in series, and n is the stage of interest.

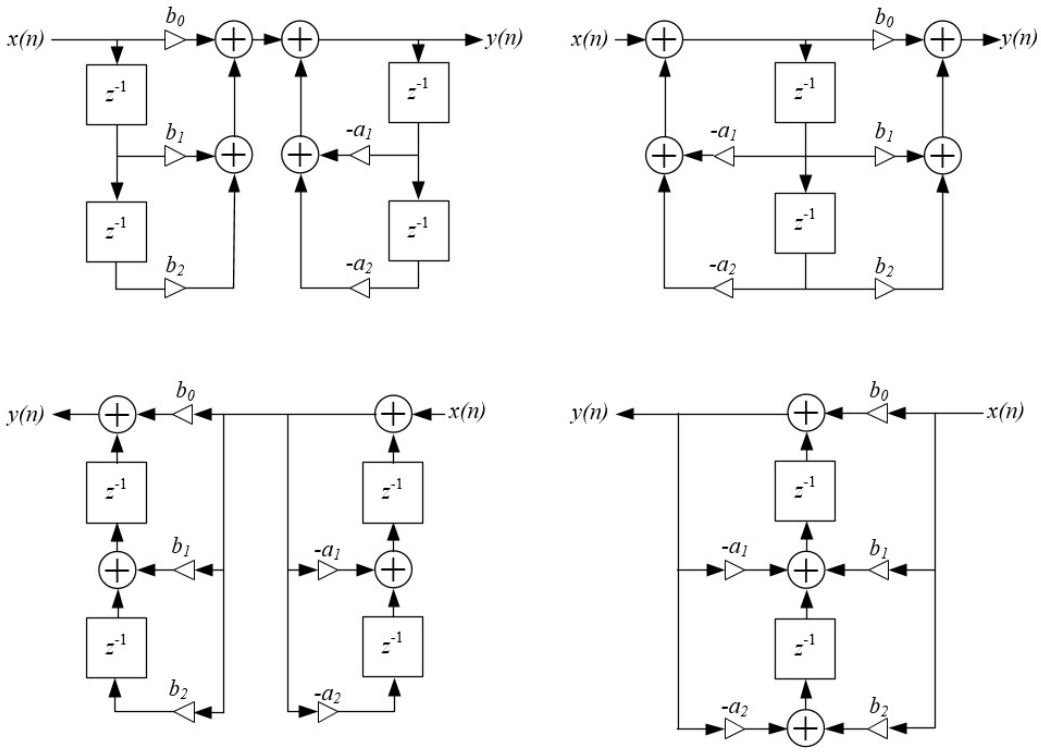

FIGURE 3.7. From left to right, Direct-Form I, Direct-Form II, the transposed variations are shown below

$$G(s) = \frac{2w_c s}{s^2 + 2w_c^2 s + w^2} \tag{3.6}$$

One key issue with the tustin transformation is that the resonant frequency has a slight shift, when designing the controller this may need to be accounted for in order for the controller to effectively attenuate the ripple power. Furthermore as seen in Fig 3.6 there is no phase shift induced at the resonant frequency when using the impulse invariance transform, and it produces a bode plot very similar to the s-domain plot of the controller. A simulation and experiment was carried out to validate the effectiveness of the transformation, however the differences in DC-link and transformer harmonics are negligible. The phase shift caused by the tustin transformation, occurs on all three-phases therefore the harmonic cancellation still occurs in the transformer windings.

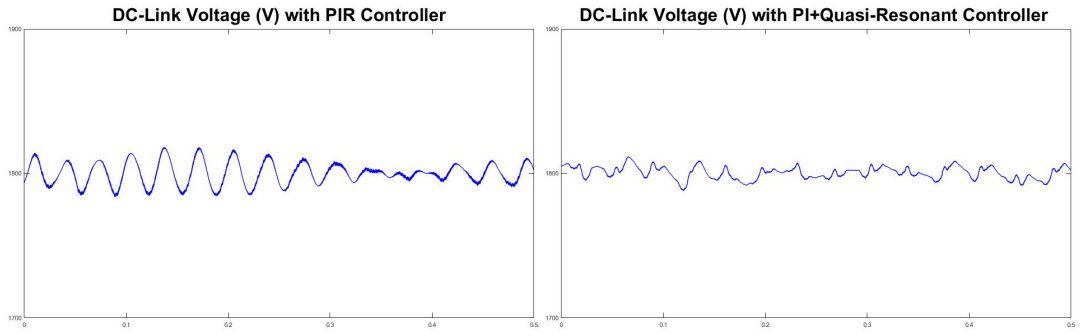

FIGURE 3.8. Resonant and Quasi-Resonant Voltage Ripple Comparison

The performance of the quasi-resonant controller in comparison to the ideal counterpart in a simulated environment, is slightly improved (reduced DC-Link ripple). Figure 3.8 shows the comparison between the controllers.

3.2.2 Experimental Setup

An experimental rig was setup to demonstrate the capability of the resonant controller seen in Fig 3.9, in a multi-level modular converter. The rig is based on Fig 3.1, there are only 2-cells present per phase and the generator input is emulated by the grid. Each cell in the experiment consists of two power module devices, one for the H-Bridge rectifier and the other for the 3 phase inverter; the power module used is the PM50RL1A120. The DC link capacitors have a total capacitance of 235 uF, additionally snubber capacitors have been added to supress voltage spikes caused by the switching devices.

A DSP (TMS320F2812) is used to process the control algorithm and generate the PWM signals, each inverter is individually controlled to achieve unity power factor operation with the resonant controller active. A set of sensor boards (seen in Fig 3.11) have been designed in order to provide feedback to the DSP.

The H-Bridge side is used to control the current and power delivered to the DC link. The PWM signals from the digital controller are passed through an intermediate stage, where a phase shift is implemented on the PWM signals. This has been done by

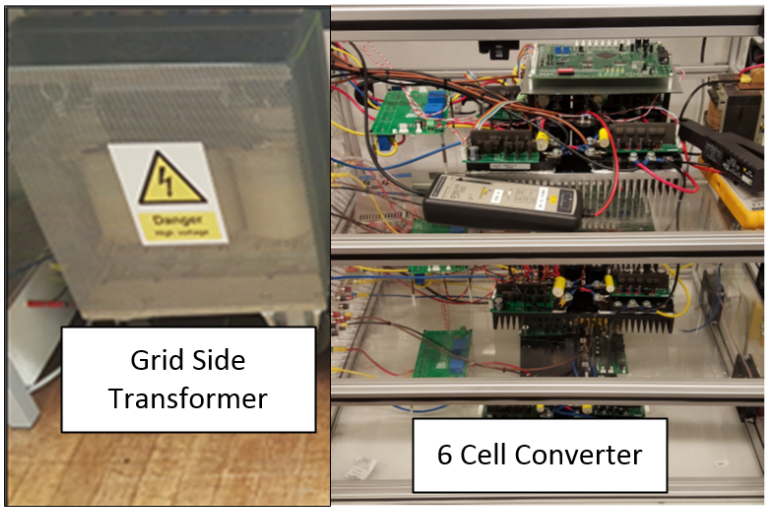

FIGURE 3.9. Experimental Rig

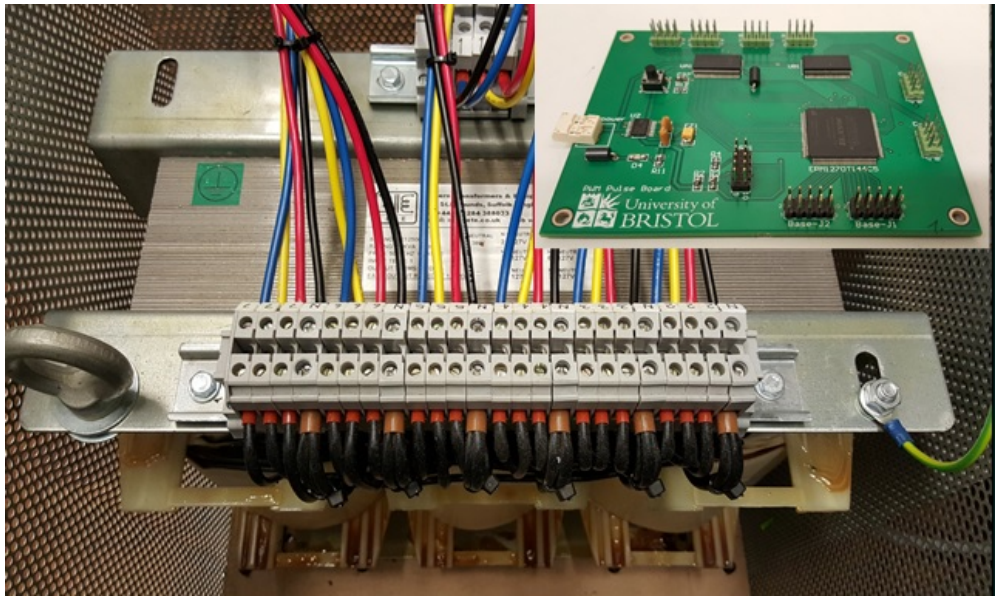

FIGURE 3.10. Transformer and CPLD

developing a CPLD board (seen in Fig 3.10), a time delay based on the clock speed is implemented to add a phase shift for the second H-bridge which is connected in series. This generates a multi-level waveform for the Cascaded H-Bridge.

The DC link voltage reference is set to 180 V, the switching frequency is set to 8 kHz

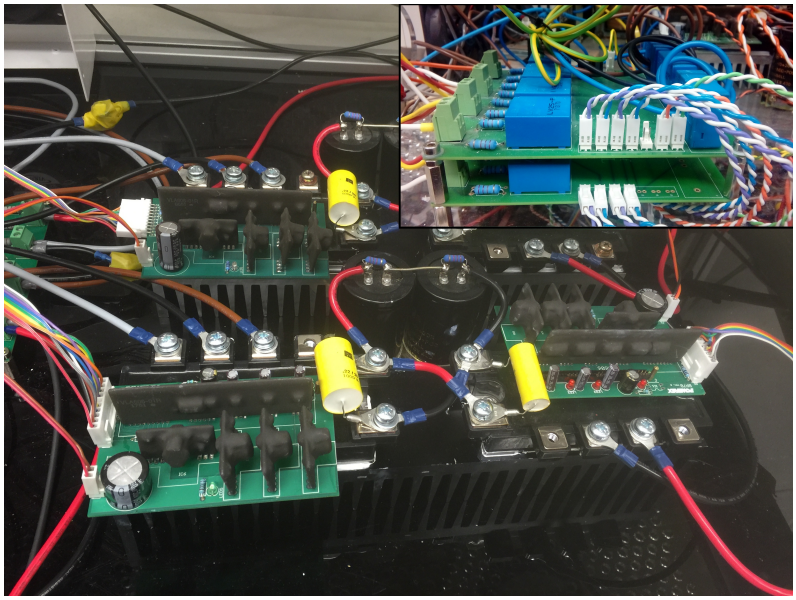

FIGURE 3.11. Close up on Two Cells of the Converter system, and in the top right the sensor board designed

and the inverter fundamental output frequency is set to 50 Hz and synchronized to the grid.

The multi-winding transformer connected to the grid-side inverter is shown in Fig 3.9 and 3.10, two of the six windings are used on the secondary side for the experiment. The transformer has a three-phase line choke connected to the primary side in order to increase the total inductance, as the experiment is scaled down (thereby reducing the transformers equivalent leakage inductance).

3.2.3 Cascaded Experimental Results

As a CPLD board was used to create the phase shift from the DSP PWM signals, an issue encountered was that when a single H-Bridge tripped a fault signal it would cause the entire H-Bridge side to shut down. This may be alleviated by modifying the CPLD code shown in the appendix to trigger an internal fault signal and shut down the PWM signals to that board only, rather than sending a fault alarm to the DSP board and shutting

down all H-Bridges. Additionally, due to the design of the CPLD board and fault signal routing it may be difficult to determine which H-Bridge is causing the fault.

When the system was being started up, and the capacitors initially being charged a large in-rush current was sometimes causing the fault signal to trip as a safety precaution. In order to counteract this the PI controller was set to have a much lower proportional gain for the first few clock cycles of the DSP, this lowered the charge rate of the capacitor thereby reducing the in-rush current.

When operating the system at higher voltages (180V DC-Link), there was spurious fault signal tripping during steady state operation. This may have been caused by noise present when the system is operating, a capacitor was added between the fault signal and ground plane. This filtered out some of the noise present, and reduced the occurrence of this issue.

Fig 3.12 shows the DC link voltage without the DC link reduction method active, and Fig 3.13 shows the DC link voltage with the controller active. The DC component of the waveform is removed to analyse the ripple in further detail. The DC link voltage ripple is reduced from approximately 36 V to below 1 V, showing the resonant controller is effectively attenuating the signal. In theory all of the harmonics present at twice the fundamental frequency should have been attenuated, however this may have not been possible due to the delay of controller and sensing equipment, in addition to other harmonics being present caused by the switching process.

The first cell inverter waveform (Fig 3.14) show that the inverter is operating near unity power factor. Figures 3.15 and 3.16 show the effect on the grid current waveform due to the control strategy. It can be seen that the current is distorted on the secondary windings, and primary. However as discussed previously the harmonics may be cancelled out in the transformer windings for a three-phase system. Therefore the grid power quality would be unaffected, although the IGBTs and transformer may incur additional

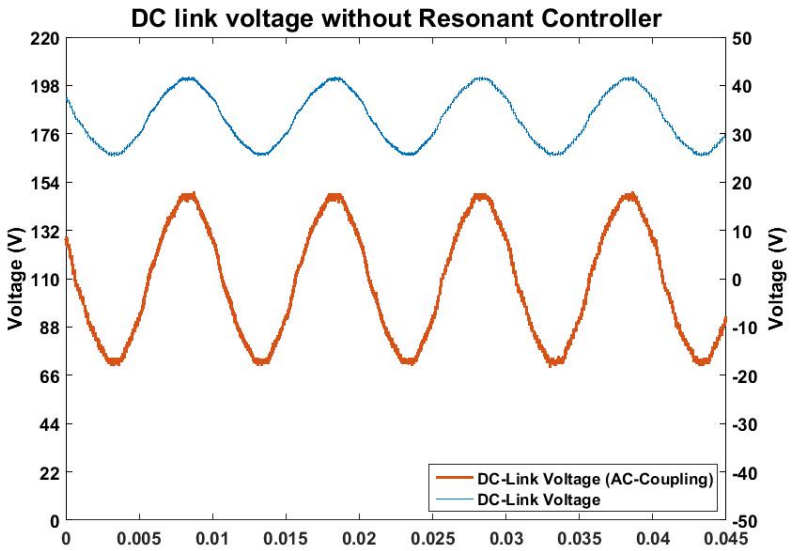

FIGURE 3.12. DC-Link Voltage with PI control

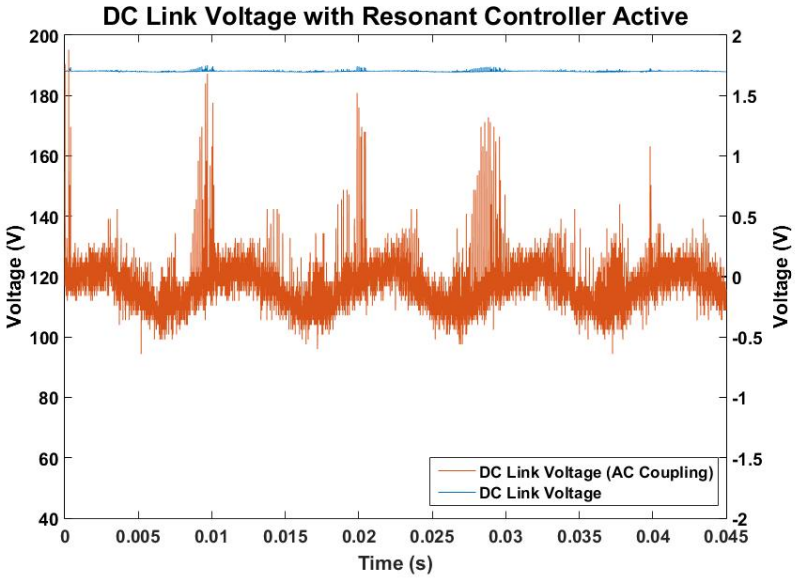

FIGURE 3.13. DC-Link Voltage with PIR control

losses. Furthermore [58] shows the effect on device temperature, the key issue would be the additional thermal cycling on the device due to the current waveform, however this would vary depending on the fundamental frequency of the system as the current harmonics would also change accordingly.

Figures 3.17 shows the Cascaded H-Bridge waveforms, it can be seen on the voltage waveform that there are 5 levels, corresponding to two stages connected in series. The current flows into the converter, which is depicted by the current waveform being 180º out of phase with the voltage waveform. The high frequency harmonics on the single-phase voltage waveform is due to the switching harmonics present at 8 kHz.

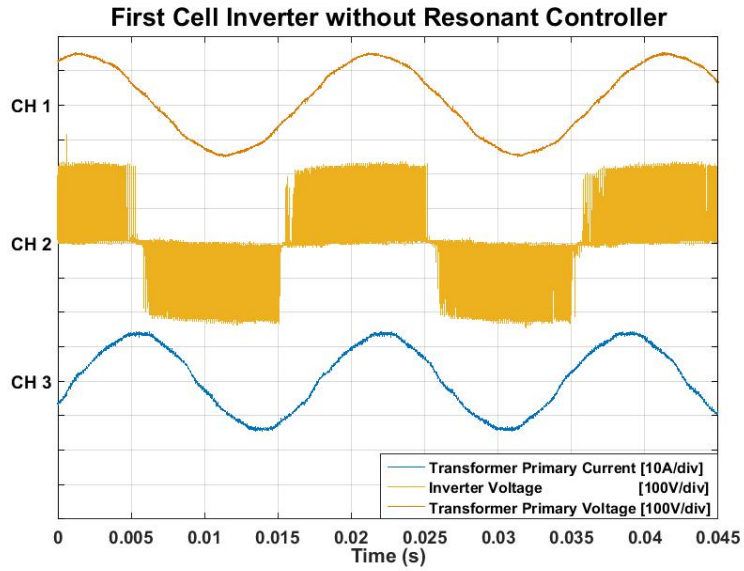

FIGURE 3.14. First Cell Inverter Waveforms

With the quasi-resonant controller actively attenuating the pulsating power generated by the H-Bridge, the effect of the capacitor value on the DC-Link voltage ripple has a much less profound effect (shown in Fig. 3.18), this may allow the use another type of capacitor that is better suited to filtering out high frequency noise generated by the switching process, and has an increased lifetime under similar operating conditions. This may allow for the frequency of maintenance on a large wind turbine to be reduced, thereby reducing the costs associated with upkeep.

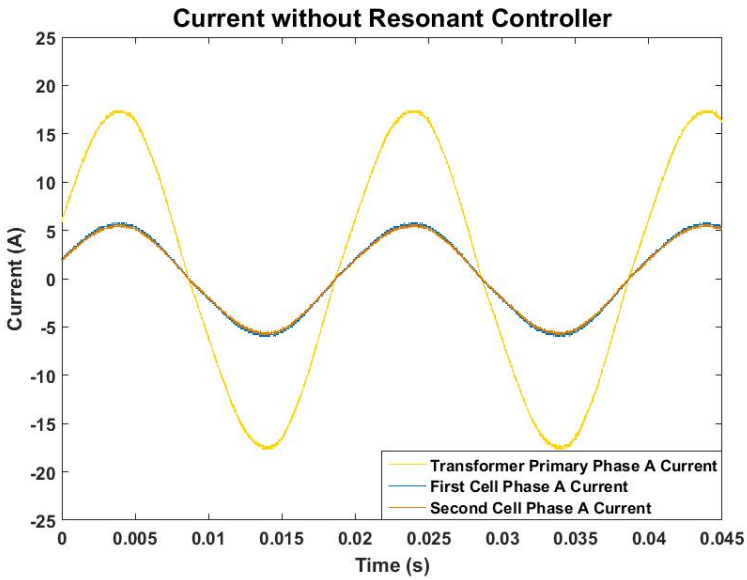

FIGURE 3.15. Transformer Current Waveforms with PI control

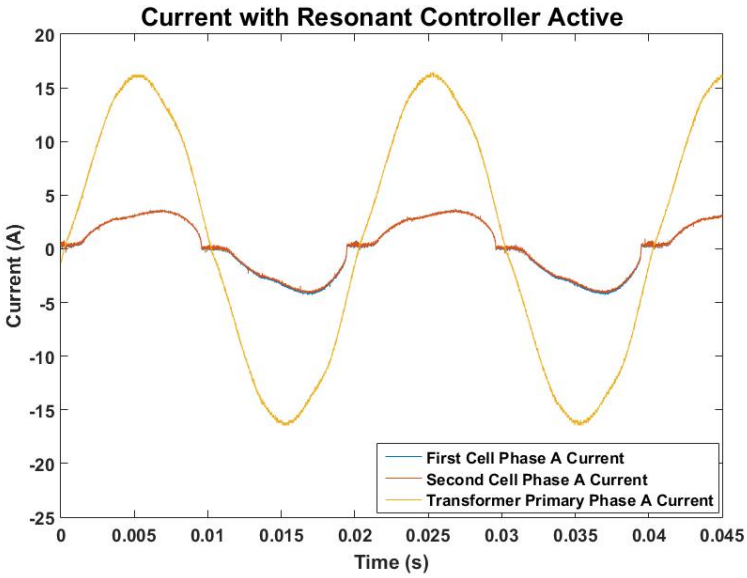

FIGURE 3.16. Transformer Current Waveforms with PIR control

3.3 Implementing semi-bridge

As a PMSG is able to operate over a range of power factors, and in a WECS power is only transferred in one direction it may be feasible to use the semi-bridge over the H-bridge.

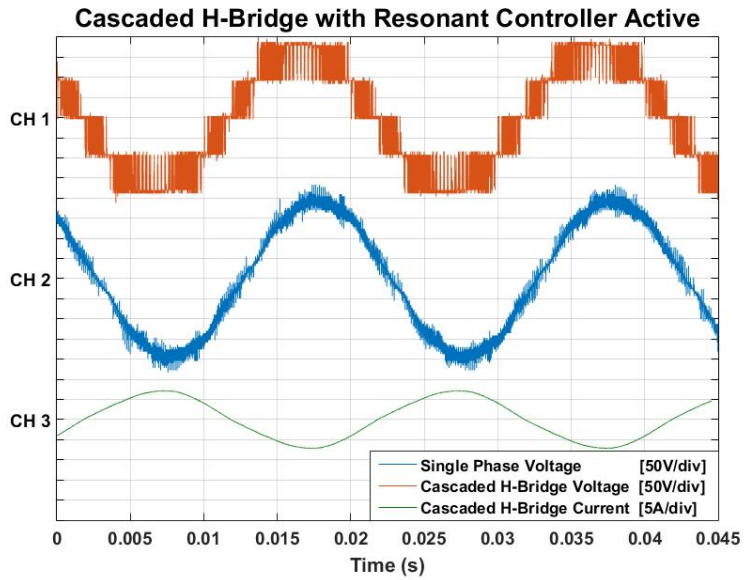

FIGURE 3.17. Cascaded H-Bridge Waveforms

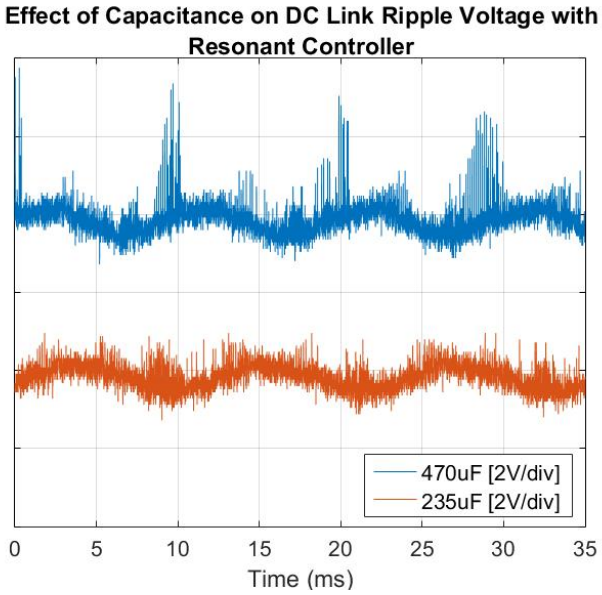

FIGURE 3.18. Effect of capacitance on DC-Link voltage Ripple with PIR control active

Furthermore when operating a generator closer to unity power factor, the losses may be lower which may allow for the generator size to be reduced. The main restriction of the semi-bridge is its capability to operate at a range of power factors.

The following paper [61] has shown that the bridgeless boost converter is capable of improving the power factor of the sources connected from 0.58 up to 0.993. The majority of PMSGs are rated to be operated between a power factor of 0.75 - 0.9, therefore the semi-bridge is suitable alternative as the reduced number of switching devices increases the robustness of the system, and reduces control complexity.

3.3.1 Simulation Results

Figure 3.20 shows the semi-bridge waveforms when the system is operating at unity power factor between the generator voltage and current, the phasor diagram is shown in Fig 3.19a. It can be seen that the system is unable to track the current reference (orange tracking yellow signal in the middle figure 3.20), this is partly due to the PI controller used to regulate the system having a slow dynamic response which is limited by the switching frequency of the system, this causes the current to have a leading phase at the zero-crossing point. Furthermore the PI controller as discussed previously only provides a high gain at DC, therefore it is not able to regulate the AC waveform adequately. In addition to this as the converter current falls to zero, the voltage across the converter terminals is still positive, this causes the converter to operate in low load conditions which may lead to discontinuous conduction mode, further adding to the distortion around the zero crossing point [62].

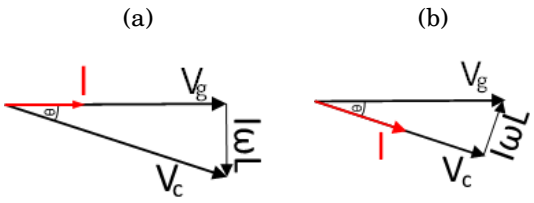

FIGURE 3.19. Left: Unity power factor between generator voltage and current, Right: Unity power factor between converter voltage and current

Fig 3.21 shows the converter operating at unity power factor between the converter

voltage and current,the phasor diagram is shown in Fig 3.19b. As the power switching devices see unity power factor, the issue of the voltage still being positive after the current falls to zero is not present anymore which substantially reduces the zero crossing error, and increases the likelihood of the converter entering discontinuous conduction mode. The issue with the control strategy is that the generator may operate at a lower power factor, therefore less active power may be transferred. The PMSG will have to generate reactive power according to its Ld and Lq inductances, which will need to be considered during the control design phase.

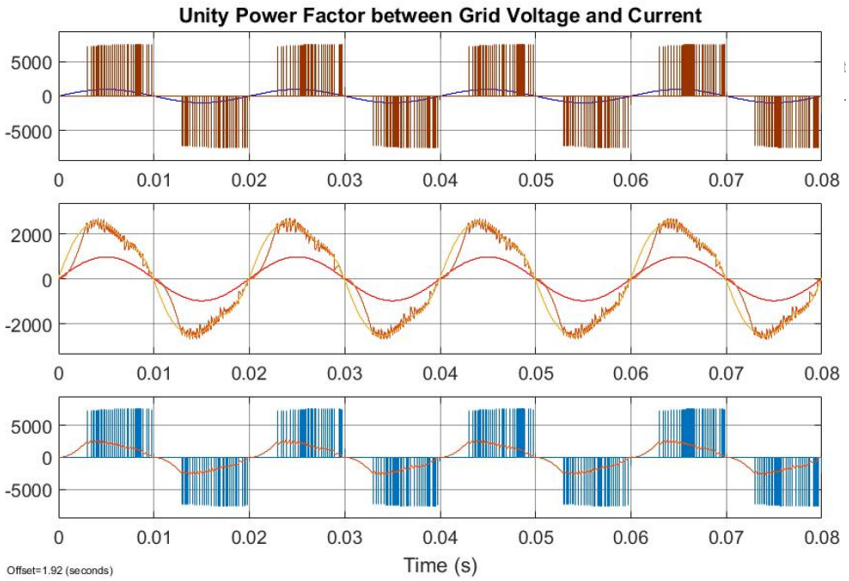

FIGURE 3.20. Top: Converter Voltage and Generator Voltage, Middle: Current Reference Tracking, Bottom: Converter Voltage and Current

The semi-bridge has been implemented into the 10 MW simulation and figure 3.23 shows the generator current during steady state operation, the current has incurred significant distortion around the zero-crossing point. This is in part due to the voltage reference used to generate the PWM signals being in phase with the PMSG voltage, instead of the voltage the devices are exposed to. This distortion present on the generator current waveform will increase the machine losses, and may increase the peak current

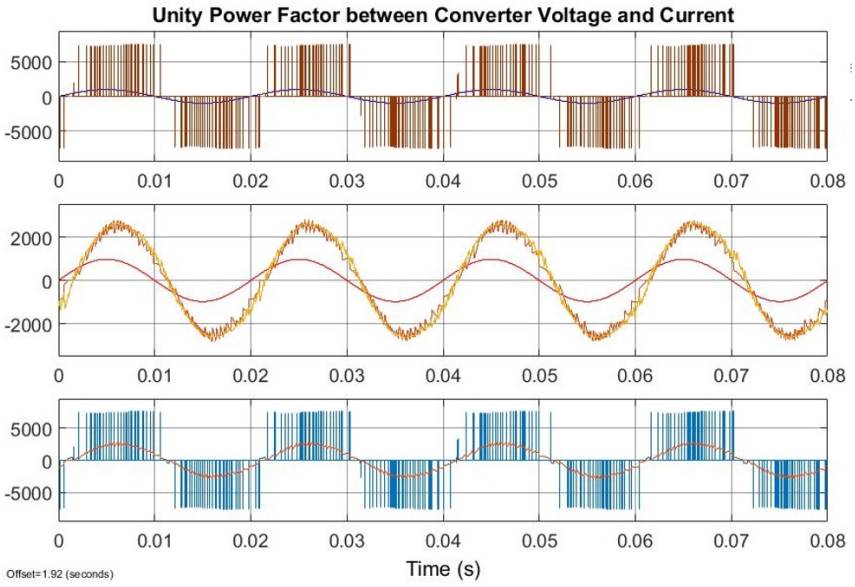

FIGURE 3.21. Top: Converter Voltage and Generator Voltage, Middle: Current Reference Tracking, Bottom: Converter Voltage and Current

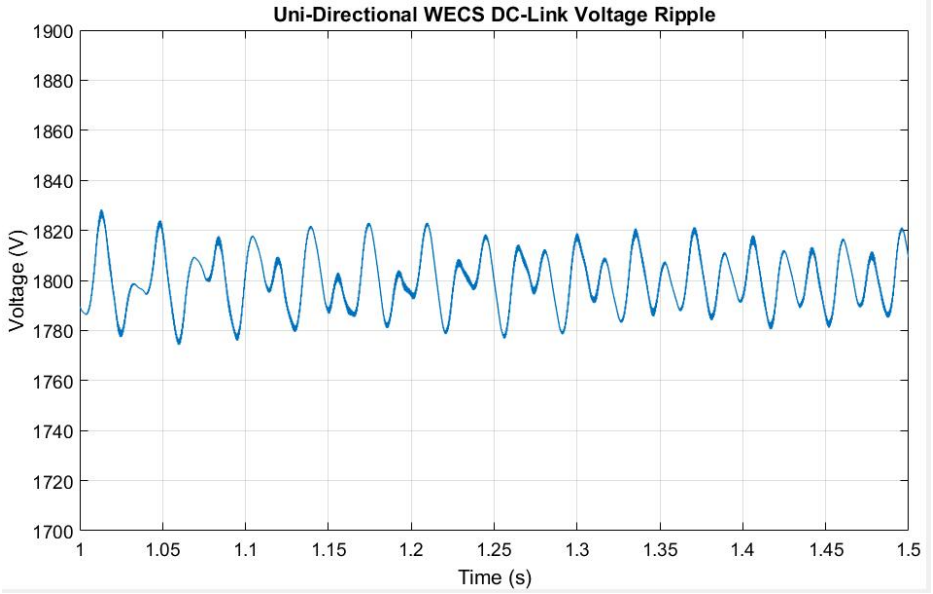

FIGURE 3.22. DC-Link Voltage Ripple with quasi resonant controller active

value in addition to the RMS stator current value. Therefore it may be more feasible to operate the PMSG at non-unity power factor in order to align the voltage the devices are exposed to with the current, in order to reduce the zero-crossing error. Figure 3.22

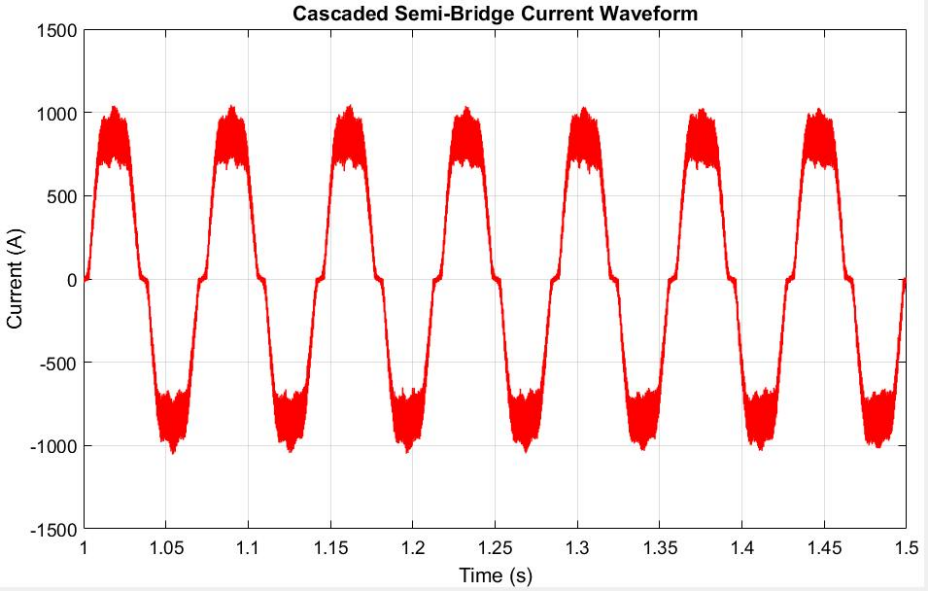

FIGURE 3.23. Cascaded Semi-Bridge Current waveform

shows the grid side converter is still able to attenuate the pulsating power produced by the H-Bridge, as the DC-Link voltage ripple is reduced in a similar manner to the quasi-resonant controller operating with the bi-directional WECS. In order to improve the current waveform, and harmonics a combination of repetitive or predictive control may be implemented, the improvement on the current waveform has been discussed in [62].

CHAPTER 4

CONCLUDING REMARKS

4.1 Conclusion

The control strategy has been successfully validated through simulation and experiments. The H-Bridge produces a low frequency ripple (twice the supply frequency) due to the low frequency supplied generated by the PMSG, this low frequency ripple requires large values of capacitance in order to filter AC component of the waveform. To achieve large values of capacitance and voltage rating, many capacitors must be connected in parallel and series. Additionally electrolytic capacitors must be used, which is an unease for reliability, and the cost/weight of the system. The capacitor bank typically occupies a third of the total converter volume. By employing the quasi-resonant control system the DC-Link voltage ripple is attenuated, and it may be possible to replace the electrolytic capacitors with a type of capacitor that has improved reliability and lifetime. Furthermore it may be possible to reduce the total capacitance of the DC-Link, as shown previously once the control system is operating the effect of the capacitance on the DC-Link voltage ripple is negligible. However the harmonics generated by the switching

process may still need to be filtered out.

The additional harmonics on the transformer secondary windings caused by the control strategy, will accelerate the rate of thermal fatigue on the power switching devices, due to the increased frequency of the thermal cycling. Additionally as the transformer incurs an additional 50% core loss [58], it must be rated to handle the increased temperature and peak current. The transformer also provides isolation, and the inductance of a large transformer may be sufficient enough to filter the waveforms in order to connect to the substation. Furthermore the pulsating power which is attenuated from the DC-Link and present on the transformer secondary windings is cancelled out in a three-phase system, providing a sinusoidal current waveform on the primary, which is proven in simulation.

The quasi-resonant controller may be suitable in real world applications, where the resonant frequency may vary slightly with noise and other disturbances. This was noticed during the experimental phase, where the controller operated in a robust manner, and required no adjustment once operating. Conversely the standard resonant controller would attenuate the dc-link ripple when the supply frequency crossed the resonant frequency briefly. Furthermore, in simulations it was found that the quasi-resonant controller attenuates the DC-Link ripple more effectively than the resonant controller. When using the control system with a PMSG and having a varying wind speed, this may cause further issues when attenuating the DC-Link voltage ripple due to the delay caused by the sensing equipment. The fundamental frequency would be detected by the sensing/control system, and the data would be used to determine the coefficients of the bi-quad filter. The quasi-resonant controller would provide more leniency for delays and sensing errors, however for a large WECS the inertia will be relatively large and the frequency will change slowly.

As the PMSG only transfers power in one direction it was validated through simu-

lation that the semi-bridge may be a feasible candidate to replace the H-bridge in the system proposed in chapter 3. In order to provide a sinusoidal current for the power switching devices, the PMSG must operate at non-unity power factor (due to machine inductances) which will incur additional losses which may require a larger generator. However the control complexity of the system is reduced and the controlled power switching device count is also reduced, this may provide a more robust system.

4.2 Future Work

Further work needs to be carried out in order to validate the uni-directional system operating in a WECS. A 3-phase experiment should be carried out with a PMSG or programmable 3-phase supply, in order to validate the current waveforms and control system. With the system setup with a PMSG it would be favourable to try mitigate the effects of the zero-crossing distortion caused on the supply waveform by investigating the use of repetitive or predictive control.

An interesting avenue for future work is the application of a single-phase to three-phase matrix converter, which would also inherit the fault tolerant operation of modular topologies. This would allow for the removal of the DC-link capacitors completely, as the converter is a AC-AC converter and there is no need for energy storage elements.

4.3 Contributions

Papers:

- Mo Al-Akayshee, Xibo Yuan - Application of non-ideal resonant controllers for DC link voltage ripple reduction in large wind turbine converters, PEMD 16.

- Qasim Al-Akayshee, Howard Neal, Adam Sartain, Stephen Reynolds, Xibo Yuan,

Mo Al-Akayshee - AN 8 MW, 3-level inverter drive based on presspack IGBT's: Design, construction and operational propulsion system, PEMD 16.

- Qasim Al-Akayshee, Howard Neal, Adam Sartain, Stephen Reynolds, Xibo Yuan, Mo Al-Akayshee - Semiconductor devices used in heavy duty industrial applications, PEMD 18.

Other:

- Engineering and Physics Sciences Research Council (EPSRC), Post-graduate summer school organising committee.
- Undergraduate electrical lab supervision/report marking, for thyristor lab.

APPENDIX A

APPENDIX A

The following figures show the MATLAB simuation layout used to generate the experimental results

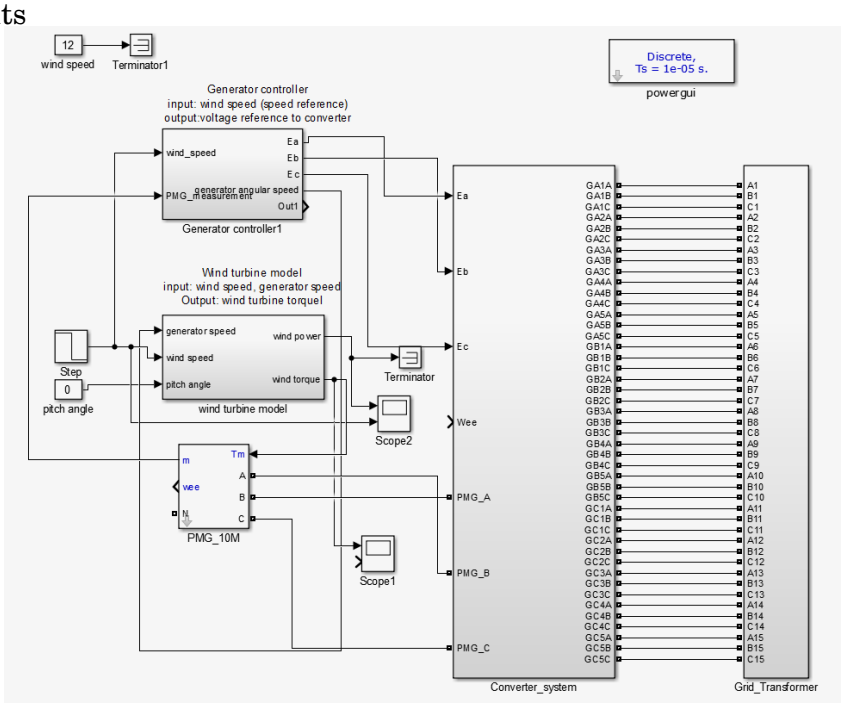

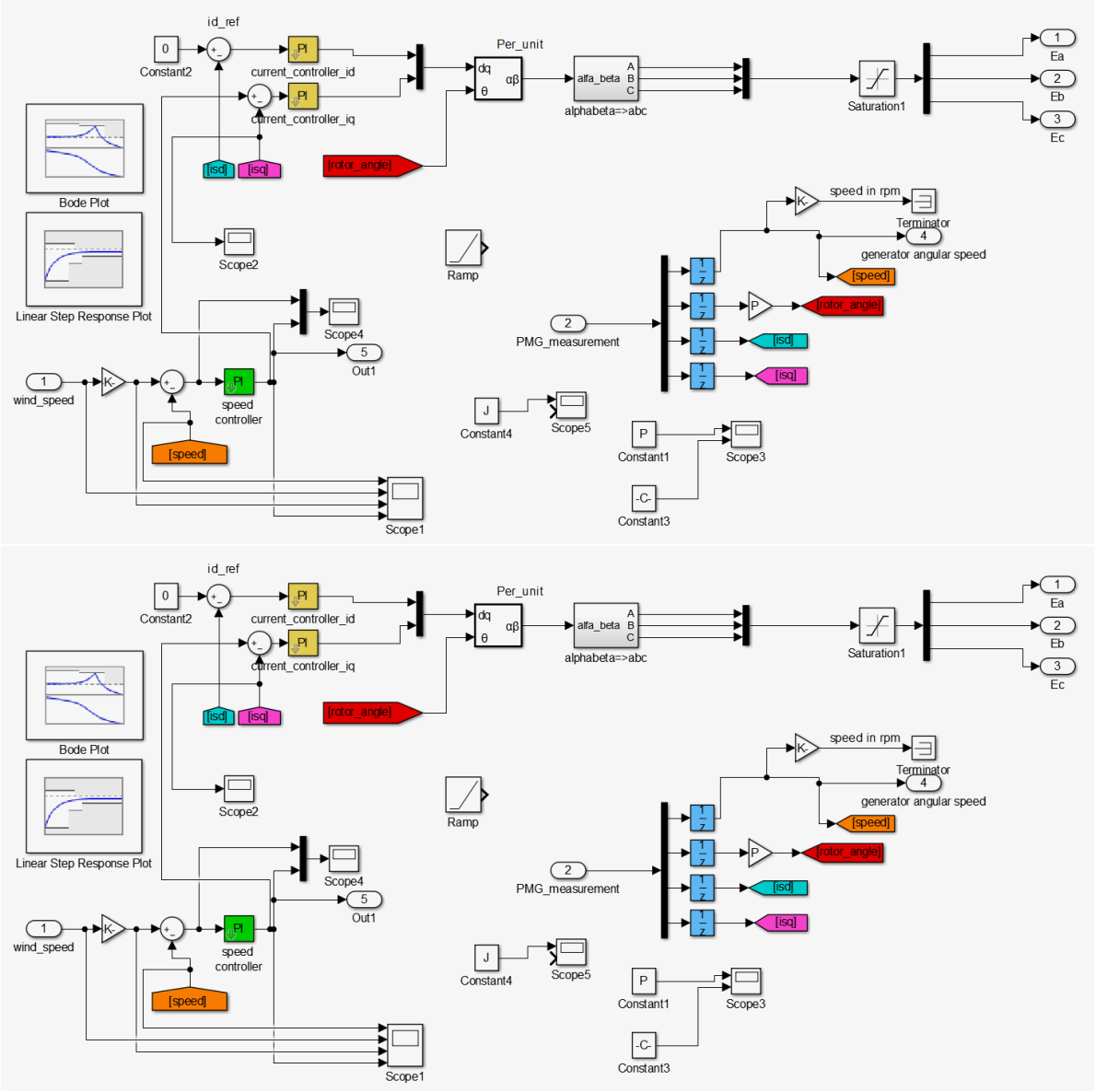

id_ref
Constant2
current_controller_id
current_controller_iq
Per_unit
dq
αβ
θ
alfa_beta
A
B
C
alphabeta=>abc
Saturation1
1
Ea
2
Eb
3
Ec
Bode Plot
Linear Step Response Plot
[isd]
[isq]
[rotor_angle]
Scope2
Ramp
speed in rpm
Terminator
4
generator angular speed
[speed]
P
PMG_measurement
Scope4
5
Out1
wind_speed
speed
controller
Constant4
Scope5
Constant1
Scope3
Constant3
Scope1

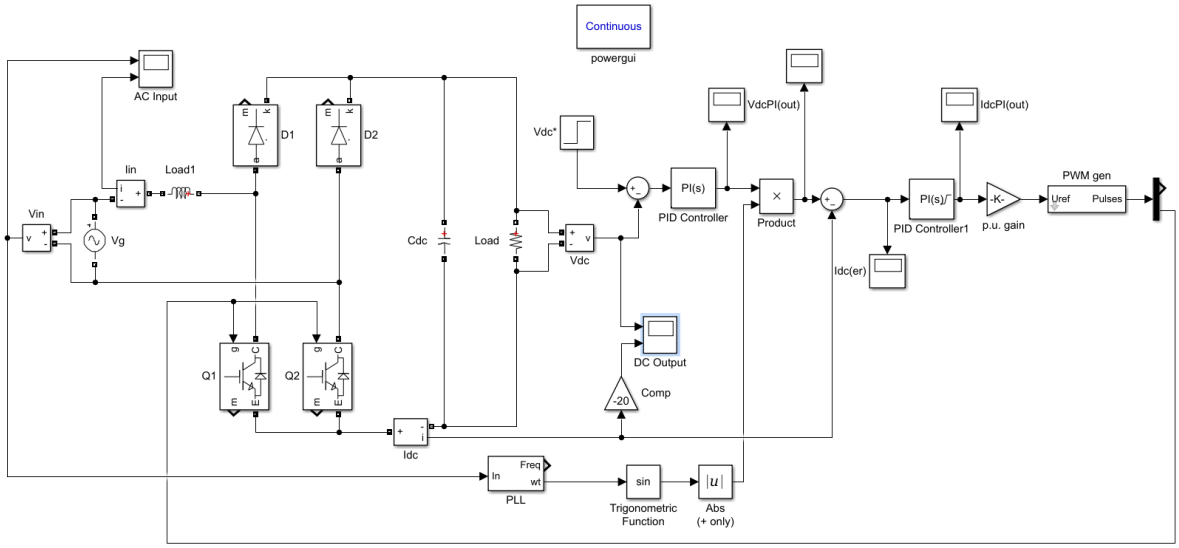

The following figures show the comparison between modulation techniques used for the PFC Bridgeless Converter. The issue with using shorted-gate modulation is that when the system is not operating at unity power factor, the controller will attempt to track the current reference with the wrong polarity.

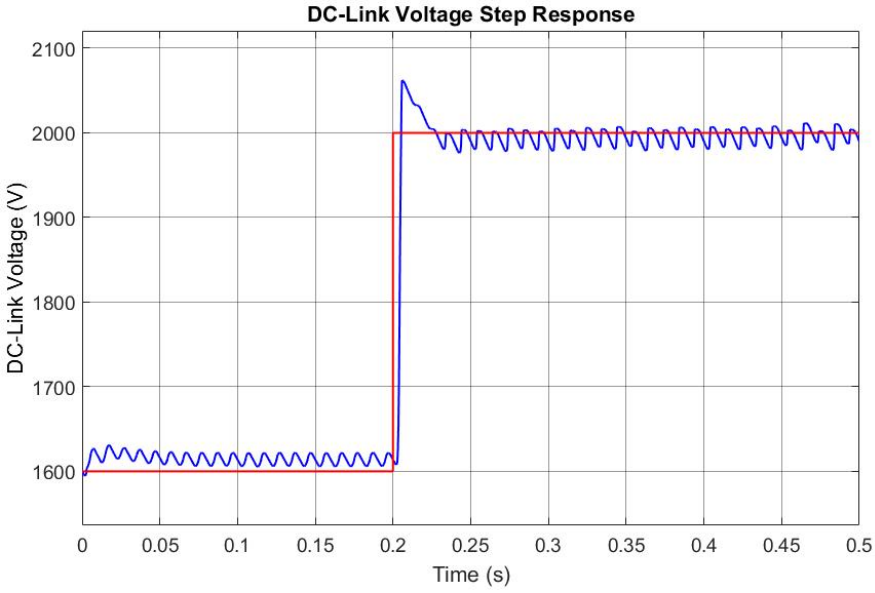

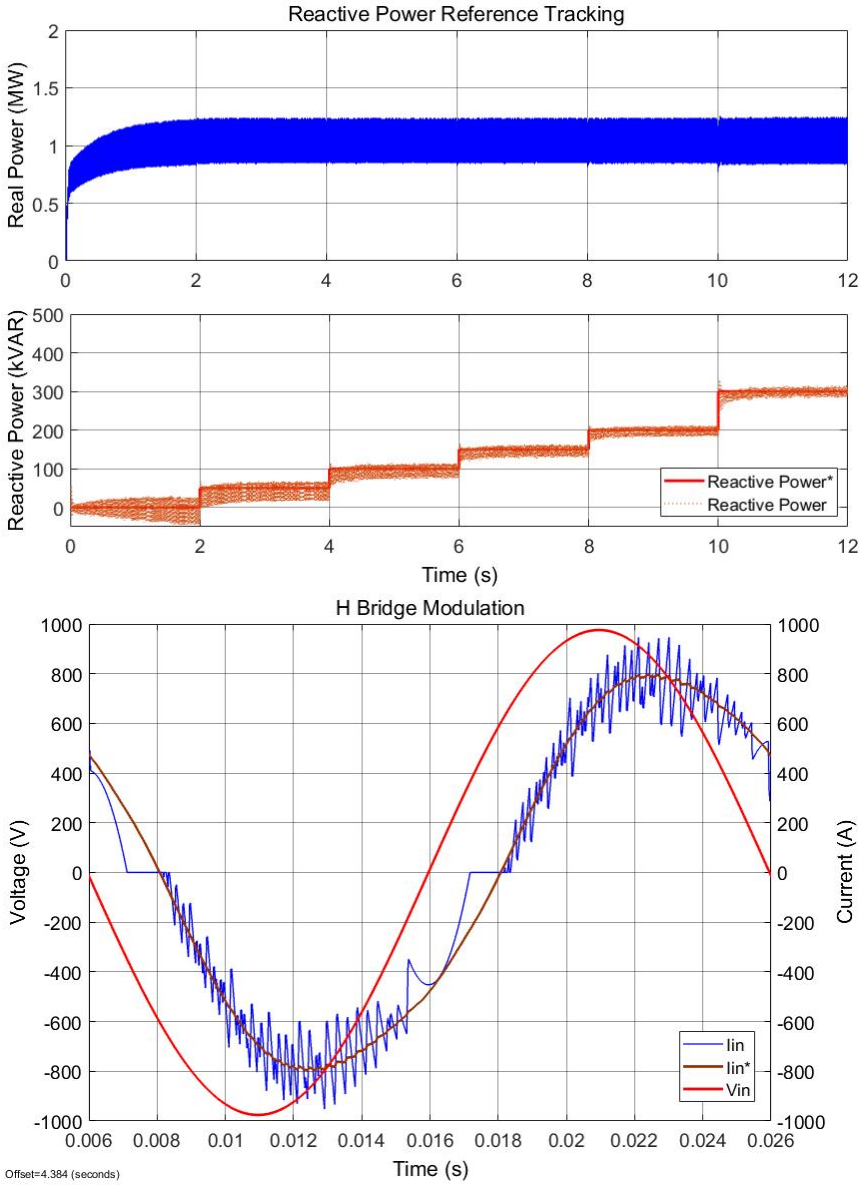
Reactive Power Reference Tracking
Real Power (MW)
Reactive Power (kVAR)
Reactive Power*
Reactive Power
Time (s)
H Bridge Modulation
Voltage (V)
Current (A)
Iin
Iin*
Vin
Time (s)
Offset=4.384 (seconds)

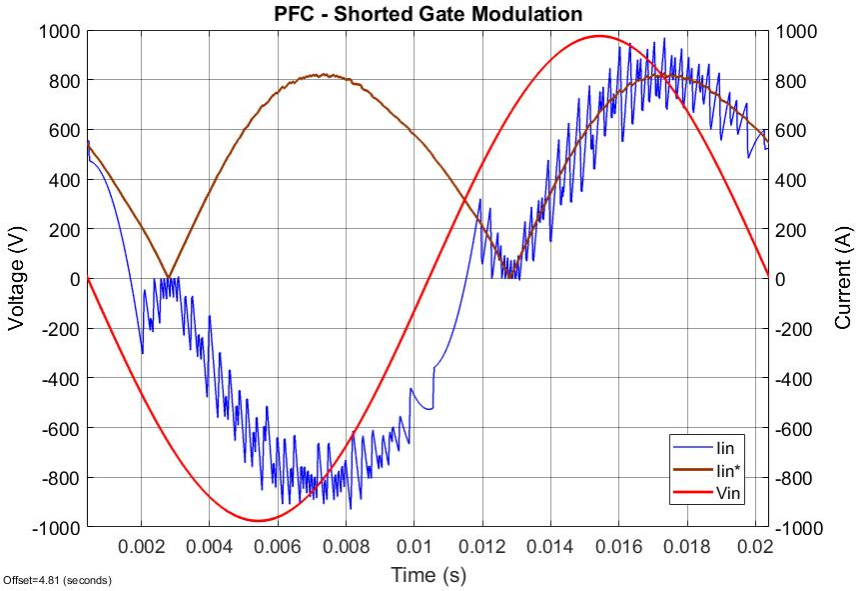

The following segment is the code used to implement the biquad filter, for the resonant and quasi-resonant controller:

```
void pr_calc (PR_Regulator *v)
{
    _iq b0;
    _iq b1;
    _iq a1;
    _iq a2;
    _iq b2;
    _iq interim=_IQ(0);

    interim = _IQcos(_IQ(0));
    b0=_IQ(1);
    b1=-interim;

    a1=_IQmpy(_IQ(2),interim);

    a2=_IQ(-1);
    b2=_IQ(0);

    v->err = v->r_ref - v->r_fdb;

    /* Integral segment */
    v->ui_delta = _IQmpy(v->Tc,_IQmpy(v->Kr,v->err));
    v->r_out= v->x_old_old+_IQmpy(b0,v->ui_delta);
    v->x_old_old=_IQmpy(b1,v->ui_delta)+v->x_old+_IQmpy(a1,v->r_out);
    v->x_old =_IQmpy(b2,v->ui_delta)+_IQmpy(a2,v->r_out);


    /* Proportional and integral repeated addition */

    if ( v->r_out > v->r_out_max )
    {   v->r_out = v->r_out_max;                /* Stop integral when saturation */
                    }
    else if ( v->r_out < -v->r_out_max )
    {   v->r_out = -v->r_out_max;               /* Stop integral when saturation */
                    }

}
```

The following code was used to convert the voltage signal from the LEM (voltage and

current sensors) into the actual value of the current and voltage read, this was done according to the sense resistor values and number of turns in the coils of the current sensors:

```
tadc.cur_param = _IQdiv(_IQ19toIQ(_IQ19div(_IQ19(2000),_IQ19(62))),_IQ(BASE_CURRENT));  //1000/62/I_BASE  1000 current ratio
tadc.cur_param = _IQdiv(_IQmpy(tadc.cur_param,_IQ(2.0)),_IQ(4.0));      //1000/62/I_BASE*2/2(4 turns)


tadc.v_param = _IQmpyIQX(_IQ12div(_IQ12(30250),_IQ12(BASE_VOLTAGE*2.5)),12,_IQdiv(_IQ(1),_IQ(62)),24);//(27000+250)/2.5/62/VDC_BASE
tadc.v_param = _IQmpy(tadc.v_param, _IQ(2.0));

tadc.v_param1 = _IQmpyIQX(_IQ12div(_IQ12(47300),_IQ12(BASE_VOLTAGE*2.5)),12,_IQdiv(_IQ(1),_IQ(62)),24);//(27000+250)/2.5/62/VDC_BASE
tadc.v_param1 = _IQmpy(tadc.v_param1, _IQ(2.0));

tadc.vp_param = _IQmpyIQX(_IQ12div(_IQ12(30250),_IQ12(BASE_VOLTAGE*2.5)),12,_IQdiv(_IQ(1),_IQ(62)),24);//(54000+250)/2.5/62/VDC_BASE

tadc.A = _IQ(0.0007326007);//3/4096;
tadc.B = _IQ(0.037932);
```

The following code is used to set the reference and feedback values for the voltage and current loops of the PI-R controllers:

```
//DC bus PI
//if (dc_pi_count>=10)
//  {
        pi_vdc.pi_fdb = tadc.VDC;
        pi_vdc.pi_ref = _IQ(0.6);
        pi_vdc.calc(&pi_vdc);
        dc_pi_count = 0;

        r_vdc.r_ref =_IQ(0.6);
        r_vdc.r_fdb=tadc.VDC;
        r_vdc.calc(&r_vdc);
//  }
//  dc_pi_count++;

//=================================================================
//id PI
    pi_id.pi_fdb = park1.de;
    pi_id.pi_ref = -(pi_vdc.pi_out+r_vdc.r_out); //_IQ(-0.4); //-pi_vdc.pi_out; //_IQ(-0.3); ////_IQ(-0.5); //  //pi_id.pi_ref = _IQ(-0.2); _IQ(0.1) for grid //
    pi_id.calc(&pi_id);

    r_id.r_ref =pi_id.pi_ref; //-pi_vdc.pi_out;
    r_id.r_fdb=park1.de;
    r_id.calc(&r_id);

////=================================================================
////iq PI
    pi_iq.pi_fdb = park1.qe;
    pi_iq.pi_ref = _IQ(0);//-0.2
    pi_iq.calc(&pi_iq);

    r_iq.r_ref =_IQ(0);
    r_iq.r_fdb=park1.qe;
    r_iq.calc(&r_iq);
```

Although there was an inbuilt protection system with the IPM (Intelligent power module), it was set to trigger at relatively high currents (50A). Therefore an alarm system has been implemented through software to have a adjustable current and voltage trigger value. The follow code shows the setting of the values:

```
protect_count ++;

    if (protect_count >5)
{
    protect_count = 6;
  if (enable_count==0)
    {
        EvaRegs.EVAIMRA.bit.PDPINTA = 1;
        EvaRegs.EVAIFRA.bit.PDPINTA = 1;
        enable_count=1;
     }


    if(tadc.VDC>_IQ(1))  //��ղ�������Ї750V
    {
        EvaRegs.COMCONA.all = 0x8000;
        EvbRegs.COMCONB.all = 0x8000;
        EvaRegs.COMCONA.all = 0x8000;
        EvbRegs.COMCONB.all = 0x8000;
        overcurrent = 1;
    }

    if ((tadc.IA >_IQ(2))||(tadc.IA <_IQ(-2)))
    {
        EvaRegs.COMCONA.all = 0x8000;
        EvbRegs.COMCONB.all = 0x8000;
        overcurrent = 1;
        current_sign=1;
    }
    if ((tadc.IB >_IQ(2))||(tadc.IB <_IQ(-2)))
    {
        EvaRegs.COMCONA.all = 0x8000;
        EvbRegs.COMCONB.all = 0x8000;
        overcurrent = 1;
            current_sign=2;
    }
    if ((tadc.IC >_IQ(2))||(tadc.IC <_IQ(-2)))
    {
        EvaRegs.COMCONA.all = 0x8000;
        EvbRegs.COMCONB.all = 0x8000;
        overcurrent = 1;
            current_sign=3;
    }
    if ((tadc.IR >_IQ(1.0))||(tadc.IR <_IQ(-1.0)))
    {
        EvaRegs.COMCONA.all = 0x8000;
        EvbRegs.COMCONB.all = 0x8000;
        overcurrent = 1;
        current_sign=4;
    }


}
```

REFERENCES

[1] M. Hoel and S. Kverndokk, "Depletion of fossil fuels and the impacts of global warming," *Research and Energy Economics*, vol. 18, no. 18, pp. 115–136, 1996.

[2] Ren21, "Renewable energy policy network for the 21st century," *Renewables 2015 Global status report*, 2015.

[3] Irena, "Renewable power generation costs in 2017," *Available at https://www.irena.org*, pp. 40–47, 2017.

[4] A. Ragheb and M. Ragheb, "Wind turbine gearbox technologies," *1st International Nuclear & Renewable Energy Conference (INREC)*, no. 1, 2010.

[5] GWEC, "Global wind energy council, global statistics," *Available at http://gwec.net/global-figures/graphs/*, 2018.

[6] M. Liserre, R. Cardenas, M. Molinas, and J. Rodriguez, "Overview of multi-mw wind turbines and wind parks," *IEEE Transactions on Industrial Electronics*, vol. 58, no. 58, pp. 1081 – 1095, 2001.

[7] T. Burton, N. Jenkins, D. Sharpe, and E. Bossanyi, *Wind Energy Handbook*. Wiley, 2011.

[8] E. Hau, *Wind Turbines*. Springer, 2013.

[9] Z. Chen, J. Guerrero, and F. Blaabjerg, "A review of the state of the art of power electronics for wind turbines," *IEEE transactions on Power Electronics*, vol. 24, no. 8, pp. 1859 – 1875, 2009.

[10] T. Ackermann, *Wind power in power systems*.
John Wiley & Sons, Ltd, 2012.

[11] F. Blaabjerg and Z. Chen, *Power electronics for modern wind turbines*.
Morgan & Claypool Publishers, 2006.

[12] D. Burnham, S. Santoso, and E. Muljadi, "Variable rotor-resistance control of wind turbine generators," *IEEE Power and Energy Society General Meeting (PES)*, 2009.

[13] S. Muller, M. Deicke, and R. D. Doncker, "Doubly fed induction generator systems for wind turbines," *IEEE Industry Applications Magazine*, vol. 8, no. 3, pp. 26–33, 2002.

[14] R. S. Semken, M. Polikarpova, P. Roytta, J. Alexandrova, J. Pyrhonen, J. Nerg, A. Mikkola, and J. Backman, "Direct-drive permanent magnet generators for high-power wind turbines: benefits and limiting factors," *IET Renewable Power Generation*, vol. 6, pp. 1–8, 2012.

[15] Ofgem.gov.uk, "New generation technologies and gb grid codes," *Available at: https://www.ofgem.gov.uk/ofgem-publications/62336/9346-gridcodechanges-pdf [Accessed 30 Oct. 2018]*, 2018.

[16] M. Tsili and S. Papathanassiou, "A review of grid code technical requirements for wind farms," *IET Renewable Power Generation*, vol. 3, no. 3, p. 308, 2009.

[17] J. Conroy and R. Watson, "Low-voltage ride-through of a full converter wind turbine with permanent magnet generator," *IET Renewable Power Generation*, vol. 1, pp. 182 – 189, 2007.

[18] F. Blaabjerg, M. Liserre, and K. Ma, "Power electronics converters for wind turbine systems," *IEEE Transactions on Industry Applications*, vol. 48, pp. 708 – 719, 2011.

[19] R. Teichmann and S. Bernet, "A comparison of three-level converters versus two-level converters for low-voltage drives, traction, and utility applications," *IEEE Transactions on Industry Applications*, vol. 41, pp. 855 – 865, 2005.

[20] J. Rodriguez, L. Franquelo, S. Kouro, J. Leon, R. Portillo, A. Prats, and M. Perez, "Multilevel converters: An enabling technology for high-power applications," *Proceedings of the IEEE*, vol. 97, no. 11, pp. 1786–1817, 2009.

[21] J. Holtz, "Pulsewidth modulation for electronic power conversion," *Proceedings of the IEEE*, vol. 82, no. 8, pp. 1194–1214, 1994.

[22] T. Meynard and H. Foch, "Multi-level conversion: high voltage choppers and voltage-source inverters," *PESC '92 Record. 23rd Annual IEEE Power Electronics Specialists Conference*, 1992.

[23] A. Nabae, I. Takahashi, and H. Akagi, "A new neutral-point-clamped pwm inverter," *IEEE Transactions on Industry Applications*, vol. 17, no. 5, pp. 518–523, 1981.

[24] S. Kouro, M. Malinowski, K. Gopakumar, J. Pou, L. Franquelo, B. Wu, J. Rodriguez, M. Perez, and J.I.Leon, "Recent advances and industrial applications of multilevel converters," *IEEE Transactions on Industry Electronics*, vol. 57, pp. 2553–2580, 2010.

[25] V. Guennegues, B. Gollentz, F. MeibodyTabar, S. Rael, and L. Leclere, "A converter topology for high speed motor drive applications," *13th European Conference on Power Electronics and Applications*, 2009.

[26] ABB, "Medium voltage drives, technologies and applications," *Available at: https://ewh.ieee.org/r3/nashville/events/2007/2007.11.12.pdf [Accessed 14 Apr. 2019]*, 2018.

[27] Industry.siemens.com, "Sinamics gm150," *Available at: https://www.industry.siemens.com/drives/global/en/converter/mv-drives/Pages/sinamics-gm150.aspx [Accessed 12 Apr. 2019]*, 2019.

[28] J. Li, S. Bhattacharya, and A. Huang, "A new nine-level active npc (anpc) converter for grid connection of large wind turbines for distributed generation," *IEEE Transactions on Power Electronics*, vol. 26, pp. 961–972, 2010.

[29] K. Wang, L. Xu, Z. Zheng, and Y. Li, "Capacitor voltage balancing of a five-level anpc converter using phase-shifted pwm," *IEEE Transactions on Power Electronics*, vol. 30, pp. 1147–1156, 2014.

[30] L. G. Franquelo, J. Rodriguez, J. Leon, S. Kouro, R. Portillo, and A. Prats, "The age of multilevel converters arrives," *IEEE Industrial Electronics Magazine*, vol. 2, pp. 28–39, 2008.

[31] C. Teixeria, D. Holmes, and B. McGrath, "Intrinsic operating limits of a single-phase semi-bridge rectifier in continuous conduction modes," *IECON 2011 - 37th Annual Conference of the IEEE Industrial Electronics Society)*, 2011.

[32] A. Gaikwad and P. Arbune, "Study of cascaded h-bridge multilevel inverter," *International Conference on Automatic Control and Dynamic Optimization Techniques (ICACDOT)*, 2016.

[33] W. Song and A. Huang, "Fault-tolerant design and control strategy for cascaded h-bridge multilevel converter-based statcom," *IEEE Transactions on Industrial Electronics*, vol. 57, pp. 2700 – 2708, 2009.

[34] L. Silva, S. Pimentel, and J. Pomilio, "Analysis and proposal of capacitor voltage control for an asymmetric cascaded inverter," *IEEE 36th Power Electronics Specialists Conference*, 2005.

[35] J. Rodriguez, J. Lai, and F. Peng, "Multilevel inverters: a survey of topologies, controls, and applications," *IEEE Transactions on Industrial Electronics*, vol. 49, pp. 724 – 738, 2002.

[36] L. Queval and H. Ohsaki, "Back-to-back converter design and control for synchronous generator-based wind turbines," *International Conference on Renewable Energy Research and Applications (ICRERA)*, 2012.

[37] D. Carlton and W. Dunford, "Multi-level, uni-directional ac-dc converters, a cost effective alternative to bi-directional converters," *IEEE 32nd Annual Power Electronics Specialists Conference (IEEE Cat. No.01CH37230)*, 2001.

[38] S. Dong, Y. Wang, and H. Li, "Coordinated control for active and reactive power of pmsg-based wind turbine to enhance the lvrt capability," *15th International Conference on Electrical Machines and Systems (ICEMS)*, 2012.

[39] C. A. Teixeira, B. McGrath, and D. Holmes, "Interleaved multicell semi-bridge rectifiers for cascaded h-bridge multilevel converters," *IEEE 7th International Power Electronics and Motion Control Conference*, 2012.

[40] B. Lu, R. Brown, and M. Soldano, "Bridgeless pfc implementation using one cycle control technique," *Twentieth Annual IEEE Applied Power Electronics Conference and Exposition(APEC)*, 2005.

[41] L. Huber, Y. Jang, and M. Jovanovic, "Performance evaluation of bridgeless pfc boost rectifiers," *IEEE Transactions on Power Electronics*, vol. 23, pp. 1381–1390, 2008.

[42] Y. Miura, S. Horie, S. Kokubo, T. Amano, T. Ise, T. Momose, and Y. Sato, "Application of three-phase to single-phase matrix converter to gas engine cogeneration system," *IEEE Energy Conversion Congress and Exposition)*, 2009.

[43] P. Wheeler, J. Rodriguez, J. Clare, L. Empringham, and A. Weinstein, "Matrix converters: a technology review," *IEEE Transactions on Industrial Electronics)*, vol. 49, pp. 276–288, 2002.

[44] X. Yuan, F. Wang, D. Boroyevich, Y. Li, and R. Burgos, "Dc-link voltage control of a full power converter for wind generator operating in weak-grid systems," *IEEE Transactions on Power Electronics*, vol. 24, pp. 2178–2192, 2009.

[45] S. Gai and M. Barnes, "Phase-locked loops for grid-tied inverters: Comparison and testing," *8th IET International Conference on Power Electronics, Machines and Drives (PEMD 2016)*, 2016.

[46] B. Popadic, B. Dumnic, D. Milicevic, V. Katic, and Z. Corba, "Tuning methods for pi controller - comparison on a highly modular drive," *2013 4th International Youth Conference on Energy (IYCE)*, 2013.

[47] R. Teodorescu, F. Blaabjerg, M. Liserre, and P. Loh, "Proportional-resonant controllers and filters for grid-connected voltage-source converters," *IEE Proceedings - Electric Power Applications*, vol. 153, pp. 750–762, 2006.

[48] B. Wu and M. Narimani, *High-power converters and AC drives*. Wiley, 2006.

[49] D. Casadei, F. Profumo, G. Serra, and A. Tani, "Foc and dtc: two viable schemes for induction motors torque control," *IEEE Transactions on Power Electronics)*, vol. 17, pp. 779–787, 2002.

[50] M. Kazimierkowski, R. Krishnan, and F. Blaabjerg, *Control in power electronics*. Amsterdam: Academic Press, 2002.

[51] H. Nguyen and D. Lee, "Reducing the dc-link capacitance: A bridgeless pfc boost rectifier that reduces the second-order power ripple at the dc output," *IEEE Industry Applications Magazine*, vol. 24, pp. 23–34, 2018.

[52] M. Mellincovsky, V. Yuhimenko, M. Peretz, and A. Kuperman, "A novel approach to active dc-link capacitance reduction for single phase power factor correction circuits," *8th IET International Conference on Power Electronics, Machines and Drives (PEMD 2016)*, 2016.

[53] W. Shi and Z. Yang, "A new method based on pir controller to reject torque and current ripple under fluctuating dc voltage for high-speed train traction drives," *15th International Conference on Electrical Machines and Systems (ICEMS)*, 2012.

[54] X. Yuan, W. Merk, H. Stemmler, and J. Allmeling, "Stationary-frame generalized integrators for current control of active power filters with zero steady-state error for current harmonics of concern under unbalanced and distorted operating conditions," *IEEE Transactions on Industry Applications*, vol. 38, pp. 523–532, 2002.

[55] P. Mattavelli, "A closed-loop selective harmonic compensation for active filters," *IEEE Transactions on Industry Applications*, vol. 37, pp. 81–89, 2001.

[56] A. Yepes, F. Freijedo, J. D. Gandoy, O. Lopez, J. Malvar, and P. F. Comesana, "Effects of discretization methods on the performance of resonant controllers," *IEEE Transactions on Power Electronics*, vol. 25, pp. 1692–1712, 2010.

[57] X. Yuan and A. Lovett, "Dc-link capacitance reduction in a high power medium voltage modular wind power converter," *2013 15th European Conference on Power Electronics and Applications (EPE))*, 2013.

[58] X. Yuan, "A set of multilevel modular medium-voltage high power converters for 10-mw wind turbines," *IEEE Transactions on Sustainable Energy*, vol. 5, pp. 524–534, 2014.

[59] D. Sera, T. Kerekes, M. Lungeanu, P. Nakhost, R. Teodorescu, and G. Andersen, "Low-cost digital implementation of proportional-resonant current controllers for pv inverter applications using delta operator," *31st Annual Conference of IEEE Industrial Electronics Society, IECON*, 2005.

[60] M. Al-Akayshee and X. Yuan, "Application of non-ideal resonant controllers for dc link voltage ripple reduction in large wind turbine converters," *8th IET International Conference on Power Electronics, Machines and Drives (PEMD)*, 2016.

[61] G. Eduardo, M. Ruiz, , M. Nicolas, L. Lezama, and J. Maria, "Modeling and development of a bridgeless pfc boost rectifier," *Revista Facultad de Ingeniería, Universidad de Antioquia*, vol. 82, pp. 9–21, 2017.

[62] D. Kim, J. Park, and K. Lee, "Scheme to improve the line current distortion of pfc using a predictive control algorithm," *Journal of Power Electronics*, vol. 15, pp. 1168–1177, 2015.